This is the author's final, peer-reviewed manuscript as accepted for publication (AAM). The version presented here may differ from the published version, or version of record, available through the publisher's website. This version does not track changes, errata, or withdrawals on the publisher's site.

# Bulk phase behaviour vs interface adsorption: effects of anions and isotopes on β-lactoglobulin (BLG) interactions

Madeleine R. Fries, Maximilian W. A. Skoda,
Nina F. Conzelmann, Robert M. J. Jacobs, Ralph Maier,
Niels Scheffczyk, Fajun Zhang, Frank Schreiber

**Published version information**

**Citation:** MR Fries et al. 'Bulk phase behaviour vs interface adsorption: effects of anions and isotopes on β-lactoglobulin (BLG) interactions.' J Coll Int Sci 598 (2021): 430-443.

**DOI:** 10.1016/j.jcis.2021.04.011

©2021. This manuscript version is made available under the CC-BY-NC-ND 4.0 Licence.

This version is made available in accordance with publisher policies. Please cite only the published version using the reference above. This is the citation assigned by the publisher at the time of issuing the AAM. Please check the publisher's website for any updates.

This item was retrieved from **ePubs**, the Open Access archive of the Science and Technology Facilities Council, UK. Please contact epublications@stfc.ac.uk or go to http://epubs.stfc.ac.uk/ for further information and policies.

# Bulk phase behaviour vs interface adsorption: Effects of anions and isotopes on BLG interactions

Madeleine R. Fries

*Institute for Applied Physics, University of Tübingen, 72076 Tübingen, Germany, email: madeleine.fries@uni-tuebingen.de*

Maximilian W. A. Skoda

*ISIS Facility, STFC, Rutherford Appleton Laboratory, Didcot, OX11 0QX, United Kingdom, email: maximilian.skoda@stfc.ac.uk*

Nina F. Conzelmann

*Institute for Applied Physics, University of Tübingen, 72076 Tübingen, Germany, email: nina.conzelmann@student.uni-tuebingen.de*

Robert M. J. Jacobs

*Department for Chemistry, University of Oxford, Oxford, OX1 3TA, United Kingdom, email: robert.jacobs@chem.ox.ac.uk*

Ralph Maier

*Institute for Applied Physics, University of Tübingen, 72076 Tübingen, Germany, email: ralph.maier@uni-tuebingen.de*

Niels Scheffczyk

*Institute for Applied Physics, University of Tübingen, 72076 Tübingen, Germany, email: niels.scheffczyk@student.uni-tuebingen.de*

Fajun Zhang

*Institute for Applied Physics, University of Tübingen, 72076 Tübingen, Germany, email: fajun.zhang@uni-tuebingen.de*

Frank Schreiber*

*Institute for Applied Physics, University of Tübingen, 72076 Tübingen, Germany, email: frank.schreiber@uni-tuebingen.de*

## Abstract

*Corresponding author, email: frank.schreiber@uni-tuebingen.de, telephone: 0049-7071-29-76058, fax: 0049-7071-29-5110

*Hypothesis*

Protein adsorption is highly relevant in numerous applications ranging from food processing to medical implants. In this context, it is important to gain a deeper understanding of protein-protein and protein-surface interactions. Thus, the focus of this investigation is on the interplay of bulk properties and surface properties on protein adsorption. It was hypothesised that the type of solvent and ions in solution should influence the protein's bulk and interface behaviour.

*Experiments*

The phase behaviour of beta-lactoglobulin with lanthanum chloride ($LaCl_3$) and iodide ($LaI_3$) in $H_2O$ and $D_2O$ was established via optical microscopy and ultraviolet-visible spectroscopy. The formation of an adsorption layer and its properties such as thickness, density, structure and hydration was investigated via neutron reflectivity, quartz-crystal microbalance with dissipation, and infrared measurements.

*Findings*

Beta-lactoglobulin does not show any anion-induced or isotope-induced effects - neither in bulk nor at the solid-liquid interface, which deviates strongly from the behaviour of bovine serum albumin. Therefore, we also provide a comprehensive discussion and comparison of protein-specific bulk and interface behaviour between bovine serum albumin and beta-lactoglobulin dependent on anion, cation, solvent and substrate properties. These findings pave the way for understanding the transition from adsorption to crystallisation.

*Keywords:* anion, isotope, bulk, adsorption, wetting, QCM-D, NR [1]

---

[1] ATR-FTIR - attenuated total reflectance Fourier-transform infra-red spectroscopy, BLG - beta-lactoglobulin, BSA - bovine serum albumin, $c^*$ - boundary between regime I and II, $c^{**}$ - boundary between regime II and III, $c_p$ - protein concentration, $c_s$ - salt concentration, $d$ - adsorbed protein layer thickness, $\lambda$ - wavelength, NR - neutron reflectivity, QCM-D - quartz crystal microbalance with dissipation, $q_z$ - momentum transfer, $\theta$ - incident angle, UV-vis - ultraviolet-visible

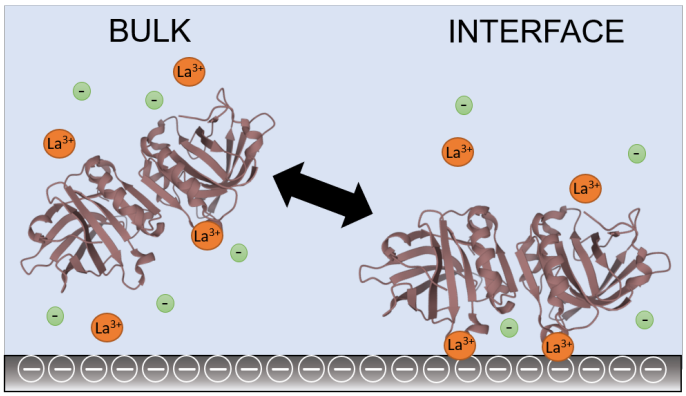


Figure 1: Graphical Abstract

## 1. Introduction

The human body is composed of roughly 16 % of proteins [1] and has to ingest ideally 180 g per day of dietary proteins to allow proper body function [2, 3]. In Central European countries, these dietary proteins originate to 28 % from meat and meat products, 28 % from milk and dairy products, 3 % from fish, 3 % from eggs and the rest is of plant origin [4, 5].

The major protein component of bovine whey is beta-lactoglobulin (BLG) [6]. The physiological concentration of BLG in cow milk varies between 4 to 20 mg/ml [7]. The main function of BLG is not yet fully established, but it was found to bind and transport small hydrophobic ligands e.g. vitamin D, cholesterol, retinol, and fatty acids [8, 6, 9, 10, 7]. Consequently, it contributes to the milk fatty acid metabolism [7], enzyme regulation, and neonatal acquisition of passive immunity [6]. Its antioxidant properties are a health benefit, especially, for milk consumers [11].

On the one hand, BLG does not occur in human milk [12], and it is not surprisingly the most common source for food allergies and (milk) intolerances in humans [13]. On the other hand, it can be used as a natural carrier for e.g. nutraceuticals due to its naturally abundance, biodegradability, and biocom-

patibility [14]. It allows the enrichment of food with nutrients through protein encapsulation, protein-based emulsions or cross-linked hydro-gels [14, 15, 16].

Due to its resistance to acid proteases [17] and gastric digestion *in vivo* [18], BLG stays intact after passing the stomach. This property is not only utilised for incorporation and delivery of nutraceuticals [15], but also for drug delivery [19, 14]. Protein-based drug delivery systems enable the transport of otherwise poorly water soluble drugs [20] such as Fenofibrate, Theophylline or Sulfamethoxazole [21, 16]. Importantly in this context, BLG can crystallise under certain conditions [22]. This facilitates new possibilities for drug purification and stabilisation through the usage of proteins [23]. One approach to control protein crystallisation, e.g. of BLG, is through the addition of multivalent salts [24, 25, 26, 27].

Salt is a natural component in e.g. milk. In food processing, salt is an important ingredient for preservation, stabilisation, and flavour enhancement [28, 29]. BLG is known to naturally bind calcium ($Ca^{2+}$) [30], which can induce a variety of phase behaviours e.g. salt-induced gelation of BLG based on hydrophobic interactions [30], which finds application in cosmetics [16]. Other multivalent salts, such as $YCl_3$, $NdCl_3$, $CdCl_2$ and $ZnCl_2$, can generate even stronger interactions than $Ca^{2+}$ and were found to induce a rich phase behaviour for BLG featuring re-entrant condensation (RC), liquid-liquid phase separation (LLPS) and protein crystallisation [31, 24, 25, 26, 27, 32]. This illustrates the complexity and variety of interactions guiding the BLG bulk phase behaviour of competing (electrostatic and hydrophobic) interactions.

Yet, not only the bulk interactions (protein-protein) have to be considered, but also possible interactions with interfaces (protein-interface). The interactions of proteins, such as BLG, with the steel or glass containers and other components must be understood to allow sterile and contamination-free food processing. The cleaning and processing of these products are based on the idea of desorption of proteins and anti-fouling surfaces [33, 34]. Certain interface properties can be favoured, e.g charged membranes in filtration systems have been shown to allow better separation of proteins [35]. In this context, the

interplay of bulk and adsorption properties is important to understand and to control.

This study, thus, focuses on BLG and the influence of different anions ($LaCl_3$ vs $LaI_3$) and solvents ($H_2O$, $D_2O$) on its bulk phase behaviour via UV-vis spectroscopy, pH, and optical microscopy measurements. In order to test the fine-tuning of interactions [36], we use chloride ($Cl^-$) and iodide ($I^-$), which are both naturally occurring in the human body [37, 38] and critical for numerous body functions [38, 39] in $H_2O$ and $D_2O$. These solvents are highly relevant for neutron scattering and vibrational spectroscopy [40, 41, 42]. New phase diagrams of BLG are established in the presence of lanthanum ($La^{3+}$) as the multivalent cation. $La^{3+}$ has a similar size to $Ca^{2+}$ [43], but induces stronger interactions due to its higher valency [44]. Thus, $La^{3+}$ offers a broader range of applications by acting as a model cation to study calcium processes [45] or as a calcium antagonist [46] in form of e.g. a neurotoxin [47].

In parallel with the bulk behaviour, its adsorption behaviour on a solid, net negatively charged, hydrophilic surface ($SiO_2$, mimicking glass) is investigated with neutron reflectivity (NR), quartz-crystal microbalance with dissipation (QCM-D), and attenuated total reflectance Fourier-transform infra-red spectroscopy (ATR-FTIR), which provides insight into the adsorbed layer thickness ($d$), hydration, roughness, and secondary structure. The adsorption process can be viewed as the primary stage of protein crystallisation, namely nucleation, at interfaces. This is part of an effort to gain a deeper understanding of protein-protein and protein-surface interactions in the presence of multivalent ions. In the following, a comparison between bovine serum albumin (BSA) (data from Ref. 48) and BLG is given, illustrating fundamental similarities and differences between the two proteins and how those affect their behaviours in bulk and at solid interfaces.

## 2. Materials and methods

### *2.1. Materials*

The materials used were purchased from Sigma Aldrich (now Merck), namely BLG with a purity of $\geq$ 90 % (product No. L3908), $LaCl_3$ with a purity of 99.99 % (product No. 449830), $LaI_3$ with a purity of 99.9 % (product No. 413674) and deuterium oxide ($D_2O$) with a purity of 99.9 % (product no. 151882). For the bulk and adsorption measurements, we prepared salt stock solutions with a concentration of 100 mM in degassed Milli-Q water or $D_2O$, as well as protein stock solutions. Most proteins containing aromatic amino acids show an absorbance maximum at 280 nm. Thus, the concentration of the protein stock solution was determined by UV-vis absorbance spectrometer measurements (Cary 50 UV-vis spectrometer, Varian Technologies, USA) scanning from 200 to 400 nm and calculating the concentration from the absorbance with the Beer-Lambert law. The extinction coefficient of BLG is 0.96 ml/(mg·cm) (Tab. 3).

### *2.2. Bulk phase behaviour*

The phase diagrams were determined at $c_p$ of 5, 20, 50, 80, and 100 mg/ml with the respective salts and in the respective solvents. $c_s$ was varied from 0 to 60 mM. The bulk samples were prepared by mixing the proteins with solvent and afterwards adding the desired amount of salt. The phase diagrams shown in Fig. 2 were determined by UV-vis transmittance measurements at low $c_s$(Fig. S2) [49] and visual inspection through the production of a dilution series shown exemplarily in Fig. S1. The phase boundary at $c^*$ is defined by the onset of turbidity correlated with a drop in transmittance. $c^{**}$ is determined by calculating the averaged value of the last turbid and the first completely re-cleared solution, which can be better understood with the transmittance progression in Fig. S2 and images of the samples in Fig. S1. Optical microscopy was used to observe the two-step LLPS formation (Fig. 3).

### *2.3. Adsorption measurements*

All adsorption measurements were performed *in situ* and the adsorption time was set to 1 h, which was sufficiently close to equilibrium conditions. All adsorption measurements were performed at $c_p$(BLG) of 5 mg/ml and at $c_s$ of 0, 0.1, 0.8, and 5 mM in $H_2O$ and/or $D_2O$.

#### *2.3.1. QCM-D*

Quartz-crystal microbalance with dissipation (QCM-D) measurements were performed with the Q-Sense Analyser of Biolin Scientific (Sweden) [50, 51, 52]. The measurements were conducted with the QSoft software and analysed with the software Qtools of Biolin Scientific. $SiO_2$-coated sensors (product No. QS-QSX303) purchased from Quantum Design (Germany) were used as substrates. Through the use of the flow cell *in situ* cleaning was facilitated with 2 % Hellmanex, ethanol, and water. By inverting the flow cell and thus placing the substrate on top of the solution, sedimentation on the substrate could be avoided. The data was analysed with the Voigt viscoelastic model since the dissipation $D$ was $< 0$ [53, 51]. The used fitting parameters for the data analysis can be found in Tab. S1.

At least three measurements per condition were performed to ensure reproducibility, stability, and accuracy of the trends found. The error bars reflect the standard deviation of those individual measurements. The systematic errors are substantially smaller than the statistical error.

#### *2.3.2. ATR-FTIR*

The absorbance measurements were performed with the Thermo Nicolet iS50 Specac Gateway ATR insert and the software OMNIC was used for data collection [54]. The detection range was set to wave numbers from 1400 to 4000 $cm^{-1}$, yet, the area of interest was defined by the amide-I band (1600 to 1700 $cm^{-1}$). The number of scans was set to 294, the resolution to 4, the gain to 1 and the aperture to 8. The substrate used was a silicon block with a native oxide

layer. Several background measurements were taken to account for the change in environment over time (data not shown)(for more information see Ref. 48).

By performing ATR-FTIR measurements, the evanescent wave penetrates through the substrate into the bulk solution. To estimate the intensity and contribution of the bulk proteins to the data collected, we flushed the Si block after adsorption with water to compare the signal of the irreversible adsorbed proteins with the signal of the protein bulk solution (data not shown). Even though this reduced the intensity, the overall shapes of the curves were the same, proving that the dominating signal came from the interface and that the protein structure was stable.

*2.3.3. NR*

Specular neutron reflectometry (NR) measurements were carried out using the PolRef time-of-flight reflectometer at the ISIS spallation source, Rutherford Appleton Laboratory (Oxfordshire, UK). A broad band neutron beam with wavelengths from 1 to 12 Å was used. The reflected intensity is measured as a function of the momentum transfer, $Q_z$ ($Q_z = (4\pi \sin\theta)/\lambda$, where $\lambda$ is wavelength and $\theta$ is the incident angle). The collimated neutron beam was reflected from the silicon–liquid interface at different glancing angles of $\theta = 0.6, 1.2$ and $2.3^\circ$ in order to cover the desired $Q$-range.

Prior to use, the $Si/SiO_2$ substrates were cleaned in piranha solution 5:4:1 ($H_2O/H_2SO_4/H_2O_2$) and afterwards put for 10 min under UV-C light for ozone cleaning. Purpose-built liquid flow cells for analysis of the silicon–liquid interface (50 x 80 mm $Si/SiO_2$ substrate) were placed on top of a variable angle sample stage in the NR instrument and the inlet to the liquid cell was connected to a liquid chromatography pump (JASCO PU-4180), which allowed the automated exchange of the solution isotopic contrast within the (3 ml volume) solid–liquid sample cell. For each solution contrast change, a total of 10 ml solution (BLG/salt/$H_2O$ or BLG/salt/$D_2O$) was pumped through the cell at a speed of 1.5 ml/min.

First, the salt/protein mixture in $D_2O$ was pumped into the cell and after

20 min of equilibration the first neutron reflectivity measurement was started. We made use of the solvent contrast effect by exchanging $D_2O$ with $H_2O$. After roughly 1 h, the cell was flushed with pure water to estimate the amount of irreversibly adsorbed proteins.

*2.3.4. NR data analysis*

Neutron data were analysed using the RasCAL2019 software package [55], which employs an optical matrix formalism (described in detail by Born and Wolf [56]) to fit layer models representing the interfacial out-of-plane structure. In this approach, the interface is described as a series of slabs, each of which is characterised by its scattering length density (SLD), thickness, and roughness. Interfacial roughness was implemented in terms of an error function according to the approach by Nevot and Croce [57], but re-sampled in RasCAL in terms of thin slabs with zero roughness, thus allowing roughnesses, which are of the order of the layer thickness. The reflectivity for an initial model based on known sample parameters, such as substrate, its oxide layer, and the solvent was calculated and compared with the experimental data. A least squares minimisation was used to adjust the fit parameters to reduce the differences between the model reflectivity and the data. In all cases, the simplest possible model (i.e. least number of layers), which adequately described the data, was selected. Error analysis of the fitted parameters was carried out using Rascal's Bayesian error algorithm [58]. The resulting plots contain fits and corresponding real space structure of the sample layer system, as well as 95 % confidence intervals (shown as shaded regions).

## 3. Results and discussion

*3.1. Bulk phase behaviour*

We investigate two salts, lanthanum chloride ($LaCl_3$) and lanthanum iodide ($LaI_3$), and their influences on the phase behaviour of BLG in $H_2O$ and $D_2O$ in Fig. 2a,b. Both salts in either solvent exhibit the same general trend showing three regimes with boundaries at the salt concentrations $c^*$ and $c^{**}$.

*3.1.1. Phase diagrams*

The general trend of the phase diagrams shown in Fig. 2 can be rationalised as follows. BLG is net negatively charged (-10 e) at neutral pH [59, 26]. This means that, without the addition of salt, repulsive forces are dominating and the samples of regime I are clear (see Fig. S1). The first phase boundary, defined by the specific salt concentration $c^*$, is reached, when the dominant interactions convert from repulsive to attractive due to multivalent cation binding and bridging [60, 61, 24]. Through the increase in salt concentration ($c_s$), protein aggregates start to form in regime II, which cause the solution to become turbid shown in Fig. S1. This can be observed and quantified either visually or by light transmittance measurements [49]. If $c_s$ is further increased, the proteins undergo charge inversion from initially net negatively to net positively charged, resulting in a decrease in attractive forces and the break-up of protein aggregates (clear solution in regime III, Fig. S1). This behaviour is called re-entrant condensation (RC) and is defined by another boundary at $c^{**}$. In the present investigation, all samples in regime II and around the phase boundaries initially form aggregates and over time undergo liquid-liquid phase separation into a dilute and a dense liquid phase. Unlike other proteins such as BSA, BLG initiates LLPS in a two-step process (Fig. 3) meaning first aggregates are formed and in a second step the system very slowly reorganises into a phase-separated solution. This behaviour is also found for other multivalent salts such as $YCl_3$ in combination with BLG [24]. In comparison with the phase diagram of BLG/$YCl_3$, the lanthanum salts induce a narrower regime II, which indicates weaker attractive forces induced by lanthanum ($La^{3+}$) being consistent with trends found for other globular proteins such as BSA [62, 63]. This can be rationalised to some degree with differences in surface charge density and polarisibility of the individual cations [62, 63].

*3.1.2. Bulk conditions for adsorption study*

Our protein concentration of interest for the adsorption study is set to 5 mg/ml, which is high enough to observe the complete rich phase behaviour

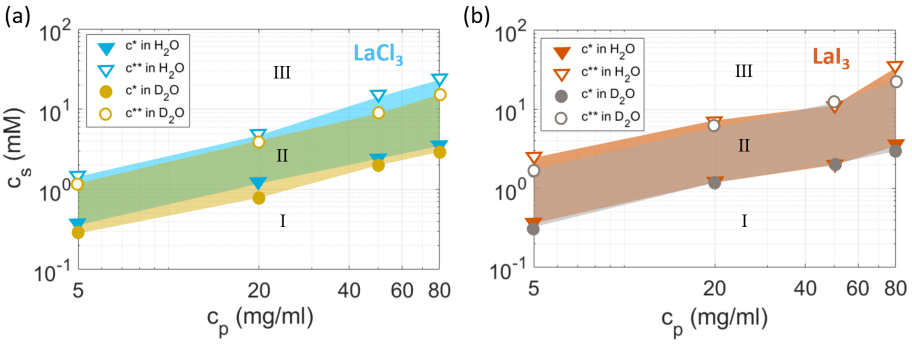


Figure 2: Phase diagrams. Phase behaviour of BLG (a) with $LaCl_3$ and (b) with $LaI_3$ in $H_2O$ (triangles) and $D_2O$ (circles), respectively. The solid markers define $c^*$, which separates regime I from regime II. The hollow markers define $c^{**}$, which separates regime II from regime III. The phase diagrams are nearly identical when comparing the different lanthanum salts and solvents. Note that the shift in phase boundaries with $LaCl_3$ between $H_2O$ and $D_2O$ might be introduced due to stock solution variations and fall within the statistical error of the measurements.

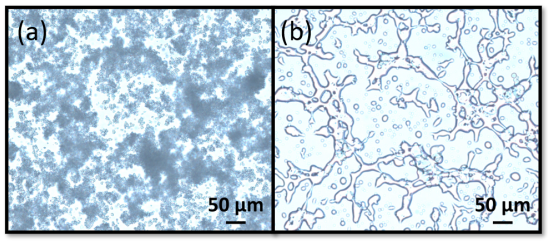


Figure 3: Two-step liquid-liquid phase separation. Microscopy images of a sample containing 20 mg/ml BLG and 2 mM $LaI_3$ in $H_2O$. (a) Aggregation directly after preparation. (b) LLPS into a dilute and a dense phase after 1 h.

Table 1: Phase boundaries. This list contains the salt concentrations corresponding to the determined phase boundaries, $c^*$ and $c^{**}$, of BLG at 5 mg/ml with $LaCl_3$ and $LaI_3$ in $H_2O$ and $D_2O$ by UV-vis transmittance measurements as shown in Fig. S2.

| | **$LaCl_3$** | | **$LaI_3$** | |
|---|---|---|---|---|
| **Solvent** | $c^*$ (mM) | $c^{**}$ (mM) | $c^*$ (mM) | $c^{**}$ (mM) |
| $H_2O$ | $0.3 \pm 0.1$ | $1.4 \pm 0.2$ | $0.3 \pm 0.1$ | $1.5 \pm 0.2$ |
| $D_2O$ | $0.3 \pm 0.1$ | $1.2 \pm 0.2$ | $0.3 \pm 0.1$ | $1.4 \pm 0.2$ |

and to be physiologically relevant, but low enough to minimise the bulk signal, and thus, bulk scattering in the neutron reflectivity measurements. The phase behaviour at $c_p = 5$ mg/ml is illustrated in Fig. S2, which shows the measured transmittance runs via UV-vis spectroscopy since the determination of $c^*$ and $c^{**}$ by visual inspection at this protein concentration is not sufficiently precise. The determined values of $c^*$ and $c^{**}$ from Fig. S2 are listed in Tab. 1 (for more information see the Experimental section). The phase diagrams of BLG, as well as the transmittance measurements, with the individual salts and solvents in Figs. 2 and S2 are quite similar to each other, yet small differences in trends can be seen. For $LaI_3$, the phase boundaries occur at slightly higher $c_s$ compared to $LaCl_3$. The same can be observed for $H_2O$ compared to $D_2O$. These differences are within the statistical error of the measurements at 5 mg/ml. Note that pH can be excluded as a dominant driving force of the phase behaviour, see Fig. S3 [64].

*3.1.3. Isotope effect in the bulk*

Importantly, the known isotope effect of BSA [65], meaning significantly stronger attractive intermolecular forces in $D_2O$ compared to $H_2O$ and thus a strong shift in phase boundaries, is not observed for BLG. This is important to mention since this means there are fundamental differences between BSA and BLG, despite both belonging to the group of net negatively charged globular proteins, than we are currently aware of (for more information see Section III.).

As a consequence, in the case of BLG, we can make use of the solvent contrast for the neutron reflectivity measurements since the difference in phase behaviour is marginal between the two solvents (more details can be found in Section II.1).

The absence of the isotope effect in BLG may be rationalised by its secondary structure and amino acid sequence. It was found that $\beta$-sheets show little to no isotope substitution, thus no significant isotope effect, whereas $\alpha$-helices contribute strongly to the isotope effect [66]. The helix formation substantially benefits, if a hydrophobic side chain is buried against the side of the helix since it facilitates structural stability [67], which illustrates the correlation between hydrophobic interactions and the presence of $\alpha$-helices. Hydrophobic interactions are enhanced in $D_2O$ due to burying of hydrophobic groups leading to a stronger protein stability in $D_2O$, [68, 69, 70, 71] and thus the combination of hydrophobic interactions and $\alpha$-helices benefit the occurrence of a strong isotope effect. Hence, a protein such as BSA being more hydrophobic than BLG (see Tab. 3) [72], as well as consisting predominantly of $\alpha$-helices is showing a strong isotope effect, whereas for BLG, the combination of fewer $\alpha$-helices (15 %) and fewer hydrophobic interactions, as well as a strong contribution of $\beta$-sheets could explain the absence of a significant isotope effect.

*3.1.4. Anion effect in the bulk*

From the literature, it is clear that BLG binds only a few small anions such as chloride [73, 74]. The ability to bind small anions can be expressed in form of the binding index $\sum(NH^+)/[\sum(COO^-) - \sum(OH)]$, which is 4.6 for BLG, but 29 for BSA in comparison [75]. This is supported by Longsworth et al. [76], who found anion binding lower by a factor of 2 for chloride and iodide to BLG, yet the number of bound anions is higher for $I^-$ than for $Cl^-$. In this context, it is useful to consider the conformation and structure of BLG. The number of free cationic vs. anionic side chains in BLG is 48 (12.9 %) to 64 (17.9 %) [77], which illustrates the protein's stronger tendency to bind cations such as $Ca^{2+}$. In fact, BLG binds twice as many $Ca^{2+}$ compared to BSA [78]. In addition, BLG tends to bind preferentially hydrophobic molecules via hydrophobic interactions

[79, 9, 80, 81]. This is further supported by the absence of fixed anions in the protein's crystal structure [24]. Thus, we can assume that little to no anions bind to BLG, which supports the anion-independent phase behaviour observed in Fig. 2 and S2.

### *3.2. Protein adsorption*

In this section, the adsorption behaviour of BLG ($c_p = 5$ mg/ml) at the solid-liquid interface is presented. For the characterisation of the adsorption layer, we use QCM-D, infra-red spectroscopy (ATR-FTIR) and neutron reflectivity (NR). Through the use of these complementary methods, we are able to gather information on the thickness, density, and hydration of the adsorption layer, as well as general trends introduced by the different bulk regimes. $SiO_2$ is used as the substrate material, which mimics a glass surface and is net negatively charged and hydrophilic [82, 83].

#### *3.2.1. Layer morphology and adsorption kinetics*

Protein adsorption at the solid-liquid interface ($SiO_2$) is measured in real-time in a flow cell using a quartz-crystal microbalance with dissipation (QCM-D) and neutron reflectivity (NR). QCM-D allows to obtain insight into the adsorbed thickness $d$ including the trapped water within in the layer and its viscoelastic properties [84, 85, 86, 87]. In addition, NR measurements at the solid-liquid interface are performed to provide information about the entire z-dependent density profile, i.e. thickness, density, roughness, hydration, and morphology of the adsorption layer. Fig. 6 shows an overview of the reflectivity curves of adsorbed BLG at different salt concentrations and salt types in $D_2O$.

**3.2.1.1. QCM-D measurements**

From the raw QCM-D data, which consists of the measured frequency $F$ and dissipation $D$, one can deduce general trends and behaviours. Exemplary data is shown in Fig. 4 and S4 for BLG with $LaCl_3$ and $LaI_3$ in $H_2O$ and $D_2O$, respectively. The weakest adsorption (smallest $\Delta F$) is measured without salt and the strongest adsorption occurs in regime II (highest $\Delta F$) at 0.8 mM for

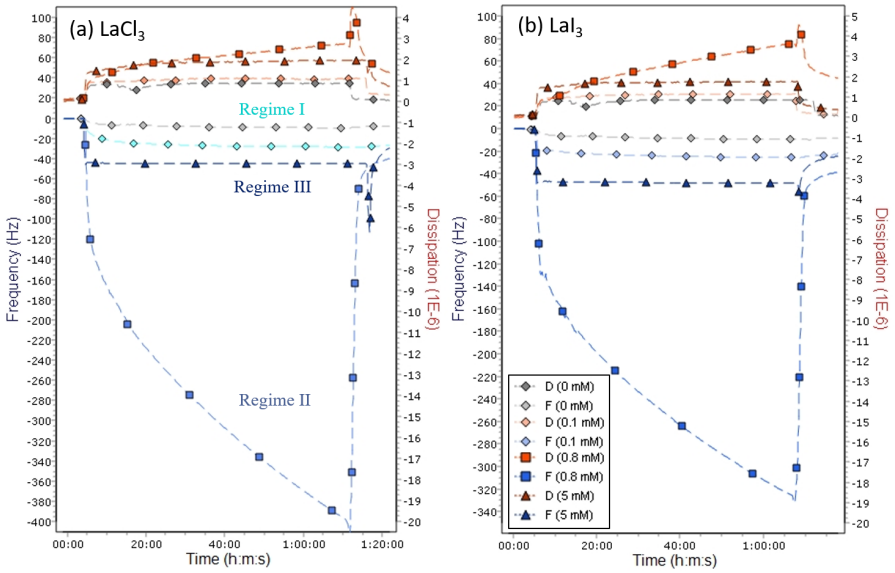


Figure 4: Raw QCM-D adsorption data. Frequency (blue) and dissipation (red) of the $9^{th}$ overtone of BLG at 5 mg/ml in $H_2O$ without salt, in regime I at 0.1 mM $c_s$, in regime II at 0.8 mM $c_s$ and in regime III at 5 mM $c_s$ adsorbed on a $SiO_2$-coated sensor in (a) with $LaCl_3$ and (b) $LaI_3$. The measurements are calibrated and started with the cell filled with $H_2O$ and after a few minutes the salt/water mixture is pumped into the cell inducing protein adsorption. After roughly 1 h, the cell is flushed with $H_2O$ to check for the reversibility of protein adsorption. Note that spikes in the raw data are induced by turning the pump on and off for solution exchange.

both salts and solvents. The change in $D$ varies from 1 $\times 10^{-6}$ to 4 $\times 10^{-6}$. Since $D$ is a measure for the viscoelastic properties, one can conclude that the protein layer formation is rather dense and stiff compared to e.g. BSA adsorbed on an interface [88, 89]. Upon rinsing, only in regime II, a significant amount of protein is flushed from the surface. Under all other conditions, most of the adsorption is irreversible, which implies strong protein-surface interactions. The adsorption process occurred on a time scale of seconds (which is not measurable by NR), except in regime II, where the layer continues to grow even after 1 h (Fig. 8).

By applying the viscoelastic Kelvin-Voigt model [51, 90, 91], the averaged adsorbed protein layer thickness $d$ over a cross-section of the substrate is calculated (details in the Experimental Methods) and shown in Fig. 5. Without salt, very little adsorption is observed ($d_{\mathrm{LaCl_3}} = 1.8 \pm 0.9$ nm) in Fig. 5a. Adding trivalent salt causes an enhancement in adsorption. At $c_s = 0.1$ mM (regime I), a slight increase of $d_{\mathrm{LaCl_3}} = 6.9 \pm 2.6$ nm can be seen in $H_2O$. By further increasing $c_s$ to 0.8 mM (regime II), thus crossing the first bulk phase boundary, strongly enhanced adsorption ($d_{\mathrm{LaCl_3}} = 60.1 \pm 11.2$ nm) is observed. This is in good agreement with enhanced adsorption found for BSA with multivalent ions [89]. This adsorption trend can be explained with the ion-activated-attractive protein adsorption model established in this context [88]. In a previous publication [89], we established that this enhanced adsorption is actually a wetting transition, i.e. the divergent layer represents a wetting layer, triggered by bulk instability due to LLPS formation. From the bulk phase behaviour, we know that BLG also undergoes LLPS formation in a two-step process at the conditions studied, which gives rise to strongly increased adsorption i.e. wetting layer illustrated in Fig. 4. At high $c_s$ (5 mM, regime III), $d_{\mathrm{LaCl_3}}$ decreases to $11.6 \pm 3.3$ nm showing re-entrant adsorption probably caused by an overcharging effect of the substrate at high $c_s$, which leads to stronger interface-protein repulsion.

For both salts in Fig. 5a, the adsorption curves lie within the error bars on top of each other, meaning the different anions ($Cl^-$ vs $I^-$) do not cause considerable

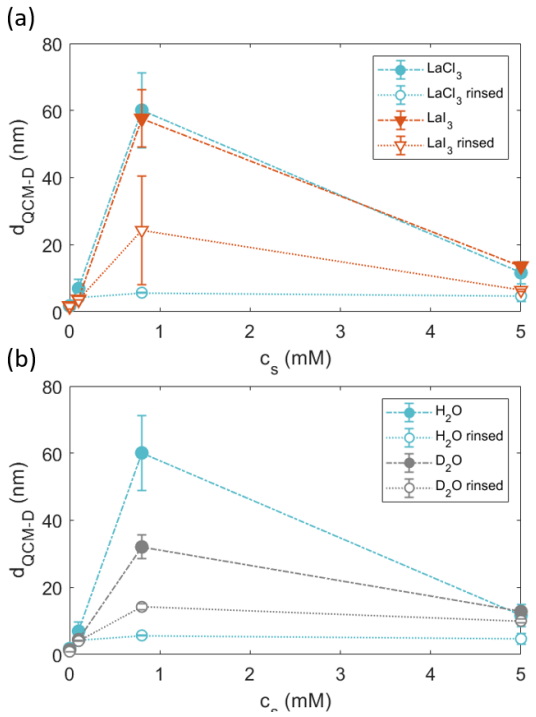


Figure 5: Solid-liquid BLG adsorption. Adsorbed layer thickness $d$ calculated with a viscoelastic model from the QCM-D data for 5 mg/ml BLG on $SiO_2$ at room temperature. (a) Influence of anion type on BLG adsorption with $LaCl_3$ (blue) and $LaI_3$ (orange) in $H_2O$. (b) Influence of solvent type on BLG adsorption in the presence of $LaCl_3$ in $D_2O$ (grey) and $H_2O$ (blue). The solid markers are samples in the salt/protein mixtures and the hollow markers label the samples after flushing the cell with $H_2O$ to check the reversibility of the adsorption process. The dashed lines are a guide to the eye.

Table 2: Fitting results of NR reflectivity data of BLG at 5 mg/ml with $LaCl_3$ and $LaI_3$. $d_{NR}$ defines the adsorbed protein layer thickness, $\sigma$ defines the layer roughness. Sub- and superscript values are parameter limits at the 95 % confidence interval (CI). Data and fits with Bayesian error analysis are shown in the Supporting Material (Figs. S5 and S6).

| | **$LaCl_3$** ($\pm$ 95 % CI) | | | **$LaI_3$** ($\pm$ 95 % CI) | | |
|---|---|---|---|---|---|---|
| $c_s$ | $d_{NR}$ (Å) | $\sigma$ (Å) | Hydr. (%) | $d_{NR}$ (Å) | $\sigma$ (Å) | Hydr.(%) |
| no salt | $28\,^{45}_{1}$ | $14\,^{22}_{9}$ | $91\,^{99}_{79}$ | $28\,^{45}_{1}$ | $14\,^{22}_{9}$ | $91\,^{99}_{79}$ |
| 0.1 mM (I) | $38\,^{45}_{31}$ | $9\,^{14}_{3}$ | $49\,^{70}_{35}$ | $39\,^{48}_{31}$ | $12\,^{18}_{3}$ | $51\,^{70}_{37}$ |
| 0.8 mM (II) | $281\,^{312}_{254}$ | $79\,^{98}_{58}$ | $47\,^{53}_{40}$ | $257\,^{288}_{234}$ | $74\,^{91}_{41}$ | $53\,^{59}_{46}$ |
| 5 mM (III) | $61\,^{69}_{52}$ | $16\,^{25}_{10}$ | $36\,^{59}_{16}$ | $65\,^{72}_{58}$ | $16\,^{25}_{11}$ | $35\,^{56}_{14}$ |

changes. This is in accordance with their similar protein bulk phase behaviour for BLG shown in Fig. 10 (note that these effects are completely different for BSA [63, 48]).

Concerning the isotope effect (solvent exchange), the raw data can be found in Fig. S4 and the analysed data is shown in Fig. 5b. The $D_2O$ data of $LaCl_3$ follows the same trend as the $H_2O$ data with little adsorption in regime I, enhanced adsorption in regime II and re-entrant adsorption in regime III. Yet in regime II, a solvent effect is observed, which was not present in the bulk behaviour. Here, adsorption was decreased by a factor of $\approx 2$ for $D_2O$. In regime II, the dominant interactions are attractive. One explanation could be that deuterium introduces stronger deuterium bonds than hydrogen bonds [92], which leads to stronger solvent-solvent interactions in $D_2O$, as well as stronger solvent-protein interactions [68], which diminish (or compete with) the attractive protein-surface interactions. In addition, the protein stability and rigidity in $D_2O$ [69] may hinder excessive adsorption and rather keeps the proteins stable in the bulk solution. Nevertheless, the differences in regime I and III are marginal, and so solvent contrast techniques could be used for NR.

#### 3.2.1.2. NR measurements

The NR measurements (Fig. 6) are in good agreement with the QCM-D and ATR-FTIR data (cf. Section II.2). By applying a one-layer model, we could

fit the SLD of our sample in Fig. 6, from which it is possible to extract the adsorbed protein layer thickness $d_{\mathrm{NR}}$, and additional structural features such as the adsorption layer roughness $\sigma$ and the hydration of the adsorbed layer. All extracted parameters and their 95 % confidence intervals are listed in Tab. 2. BLG is a rather small protein ($R_{\mathrm{H}} = 2.35$ nm) and has a high charge density, which leads to strong repulsive forces. Thus, without salt, the NR fits show a highly hydrated (low volume fraction) protein layer with a thickness of 28 Å and a hydration of 91 %. At low $c_s$, a small bump is visible at $Q_z = 0.1$ Å$^{-1}$, indicating the formation of a distinct and denser layer of 38 Å with a hydration of 49 %. In both cases (no salt and 0.1 mM), a two-layer model was also tested, but discarded, since the error analysis did not justify the assumption of two distinct layers. Thus, in regime I, BLG forms (less than) a monolayer, the density (or volume fraction) of which increases, as salt is added. The roughness of the layer at 0.1 mM salt concentration is 12 Å, which indicates a rather ordered layer.

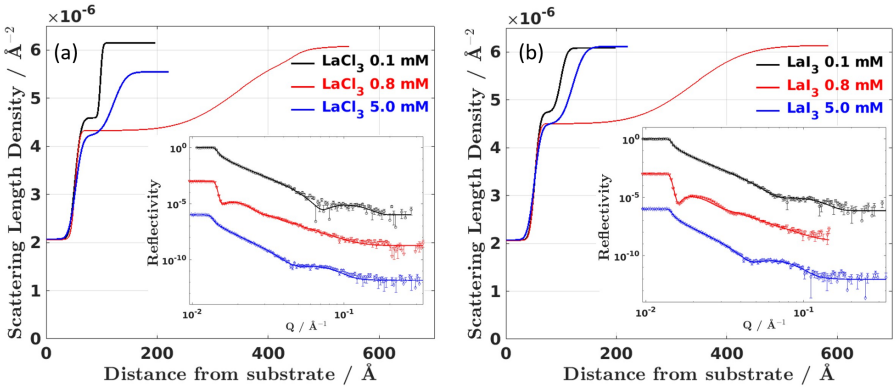


Figure 6: Neutron reflectivity data in $D_2O$ (insets) and derived scattering length density (real space) profiles of 5 mg/ml BSA adsorbed to $SiO_2$ in the presence of (a) $LaCl_3$ and (b) $LaI_3$. Note that the $H_2O$ reflectivity curves are not shown for better clarity, but can be found in the Supporting Material (Figs. S5 and S6).

In regime II, enhanced adsorption is observable (see Fig. 7 and 8). For regime II, the best fits of the NR data yield a two-layer configuration, with the first layer being 281 Å thick with a lower hydration of 47 %, and a second, much sparser

layer having a thickness of 98 Å with a hydration of 92 %. The roughness of the first layer is rather high (47 Å), suggesting a much more disordered layer, possibly caused by the adsorption of aggregates from solution, rather than growth arising from adsorption of individual proteins, which is consistent with a wetting transition [89] and the consequential morphology change. It is interesting to note that the hydration of the first layer does not suggest any significant denaturation of protein at the interface, which is also in agreement with the ATR-FTIR analysis (shown in the next Section II.2). In agreement with ellipsometry and ATR-FTIR, we detect re-entrant adsorption and diverging thickness in regime II.

In absolute numbers, the overall trend is very clear. There was nearly no difference between protein adsorption in the presence of $LaCl_3$ and $LaI_3$. The thicker the adsorption layer becomes, the rougher it becomes, while the hydration is around 50 % for regimes I and II, but drops to about 35 % in regime III (with larger error bars). This reduced hydration is below that of a minimally solvated protein layer and potentially suggests some denaturation. This, however, was a small effect and could not be confirmed in the ATR measurements.

A hydration of around 50 % indicates that the protein layer is densely packed. This might be rationalised with BLG naturally occurring as a dimer [93], as well as its ability to crystallise. Sufficiently close proximity between proteins is required to start the nucleation process.

In order to assess the accuracy and precision of the created fitting model, we performed a Bayesian error analysis. The error intervals given in Tab. 2 are obtained from this analysis and denote 95 % confidence intervals. An example is shown in Fig. 7 of 5 mg/ml BLG with no salt and 0.1 mM $LaCl_3$. The shaded areas depict the possible fit and real space profile ranges within the 95 % confidence interval. Although the 95 % confidence interval is broader than usual, the adsorption trend and structural changes can be clearly determined.

Here, one can see the benefit of using the solvent contrast of $D_2O$ and $H_2O$ due to the different shape of the reflectivity curve and $D_2O$ having a critical edge. This is based on their different SLDs and allows tailored data analysis.

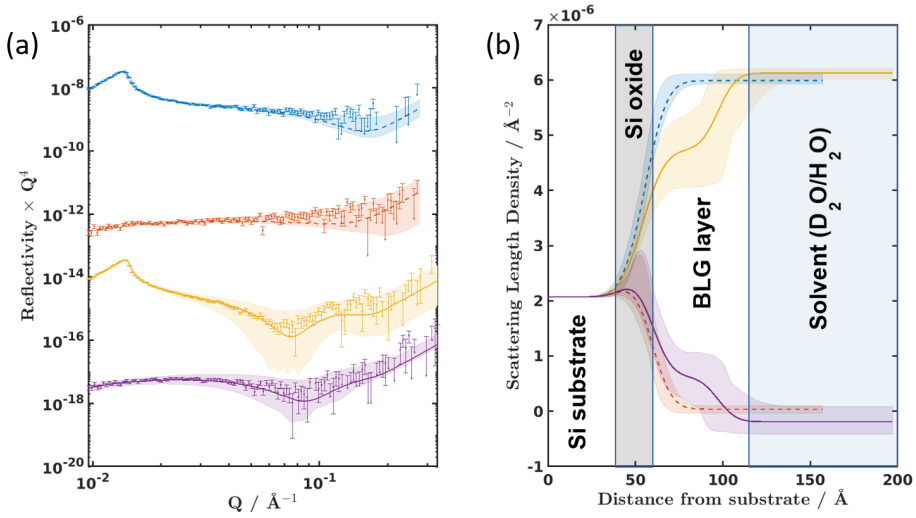


Figure 7: Bayesian Error Analysis. Fit quality of model showing 95 % confidence intervals (shaded regions) of (a) the generated reflectivity curves and (b) the resulting scattering length density profiles. The data shown is collected with a sample of BLG at 5 mg/ml without salt (blue and red, dashed) as a reference and regime I, i.e. 0.1 mM $LaCl_3$, (yellow and purple, solid), in $D_2O$ and $H_2O$, respectively.

Note that the QCM-D data shows reduced protein adsorption in regime II in $D_2O$ compared to $H_2O$, which should be kept in mind, when looking at the NR measurements in regime II, in which the reflectivity curves in $D_2O$ and $H_2O$ are assumed to resemble identical samples. Yet, due to the strongly enhanced adsorption in both solvents compared to the other regimes does not detract from the overall adsorption trend.

Based on the QCM-D results, which show a continuing growth in regime II even after more than 1 h (Fig. 4), we followed the adsorption kinetics of the $LaCl_3$ sample in regime II for more than 2 h (Fig. 8). We observe an enhanced and growing adsorption layer of almost constant density and increasing roughness. As can be seen, the data in $D_2O$ shows a fringe and peak at relatively low $Q$, corresponding to a layer thickness of approximately 200 Å. After 2 to 3 h, the layer thickness increases up to approximately 300 Å. This is consistent with previous findings in BSA showing a wetting transition at the interface for samples

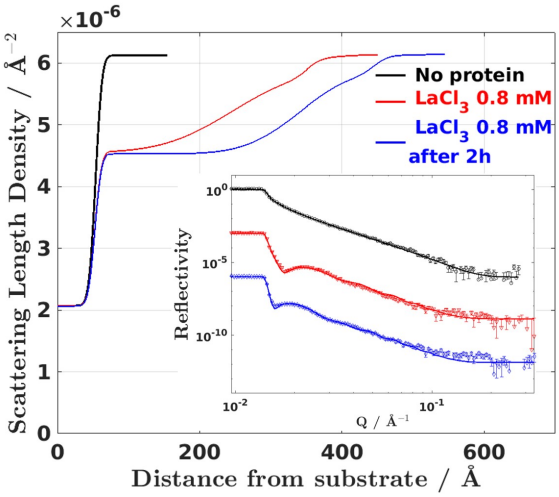


Figure 8: Wetting layer growth in regime II. Time-dependent reflectivity curves of 5 mg/ml BLG at 0.8 mM $LaCl_3$ in $D_2O$. The adsorption layer continuously kept on growing in thickness and in density (red after injection, blue after 2 h).

in the LLPS regime [89] and emphasising its universality.

### *3.2.2. Layer stability via ATR-FTIR*

Attenuated total reflection Fourier-transform-infra-red spectroscopy (ATR-FTIR) is used to study the layer stability and structural arrangement after protein adsorption on the solid-liquid $SiO_2$ interface. IR absorbance measurements are able to provide insight into the secondary structure, which can be inferred from the amide-I band at 1600 to 1700 $cm^{-1}$. In Fig. 9, the ATR-FTIR spectra of BLG with different concentrations of $LaCl_3$ and $LaI_3$ are plotted in $H_2O$. The peak maxima at 1632 $cm^{-1}$ correlate with the presence of $\beta$-sheets, which make up 54 % of the BLG structure [94, 95]. We can thus conclude that the main protein structure seems to be largely intact and is not affected by the addition of multivalent salts or adsorption to a solid interface.

The $LaCl_3$ and $LaI_3$ data in Fig. 9 show the same intensities in absorbance and curve shapes in the individual regimes. No salt-dependent structural changes can be found. Another interesting observation is the change in absorbance over

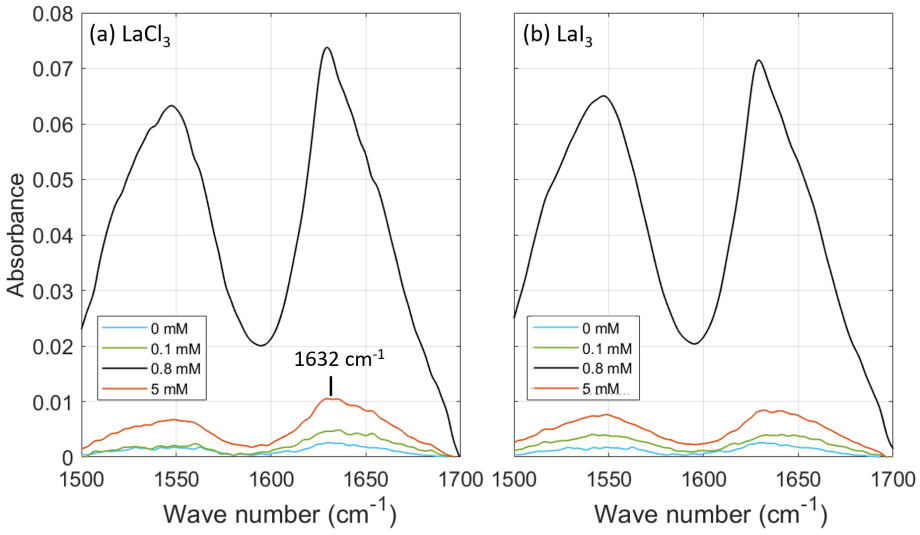


Figure 9: Interfacial structure stability of BLG. ATR-FTIR absorbance measurements of BLG at 5 mg/ml in $H_2O$ with (a) $LaCl_3$ and (b) $LaI_3$ at different $c_s$ adsorbed on $SiO_2$ are presented. The shapes of the curves are similar to each other under all conditions meaning the same intact protein structure can be assumed.

the different regimes, which does directly correlate with the amount of proteins adsorbed to the interface. Again, re-entrant adsorption (red curve) and enhanced adsorption (black curve) in regime II can be observed, which reflect the findings of the QCM-D data in Fig. 5a and the NR data in Tab. 2.

### *3.3. Discussion of differences between BSA and BLG*

This investigation provides insight into the dependence of BLG on different parameters, which guide its bulk phase behaviour and adsorption behaviour. In order to understand better what is protein-specific, we compare BLG to BSA, which is the most commonly used protein. In this section, we summarise and discuss certain protein-specific behaviours found (Tab. 4) and try to relate those to specific protein properties listed in Tab. 3. We note, though, that of course the resulting behaviour is always the result of a complex interplay of several factors, so that typically there is no simple correspondence between a certain effect and only one parameter.

Table 3: Protein properties. Relevant parameters, which influence the possible interactions of BSA and BLG.

| **Parameter** | BLG | BSA |
|---|---|---|
| Hydrodynamic radius at pH=7 [96, 97] $R_H$ (nm) | 2.35 | 3.5 |
| Molecular weight (monomer) [98, 97] $M_w$ (kDa) | 18.3 | 66 |
| Isoelectric point [59, 99] | 5.2 | 4.6 |
| Net charge at pH=7 [59, 99] ($e^-$) | -10 | -10 |
| Gibbs free energy of transfer from water [72] $\Delta G$ (kcal/mol) | -1.7 | -5.1 |
| Extinction coefficient [100] $\varepsilon^{279\ \mathrm{nm}}_{1\ \mathrm{g/L}}$ (ml/(mg·cm)) | 0.96 | 0.667 |
| Anion binding index [75] $\sum(\mathrm{NH}^+)/[\sum(\mathrm{COO}^-) - \sum(\mathrm{OH})]$ | 4.6 | 29 |
| Secondary structure [95, 101] | $\alpha \sim 15\%$ | $\alpha \sim 66\%$ |
| | $\beta \sim 54\%$ | $\beta \sim 21\%$ |
| Natural configuration at pH=7 [32, 102] | dimer | monomer |

First, we focus on similarities and differences in the *bulk* phase behaviour of BSA and BLG:

- **Role of cations.** Our group investigated two multivalent cations, $La^{3+}$ and $Y^{3+}$, and their role on the BSA and BLG phase behaviour. In a previous publication, Matsarskaia et al. [62] established the influence of $La^{3+}$, $Y^{3+}$, and $Ho^{3+}$ on the BSA phase behaviour and Zhang et al. [24] on the phase behaviour of BLG with $YCl_3$. Depending on the cation size, thus its surface charge density and polarisability, its influence on the dominant bulk interactions can be estimated. The higher the surface charge density of the cation, the stronger protein-protein forces are expected, but there are also non-trivalent entropic contributions, which are difficult to estimate [103, 104].

- **Liquid-liquid phase separation.** We find that LLPS forms in one step for BSA and within two steps for BLG (first aggregates in Fig. 3a). LLPS is temperature-driven. The different behaviours are influenced by entropy

and enthalpy of mixing and de-mixing [105], which results in a lower critical solution temperature (LCST) for BSA [60] and an upper critical solution temperature (UCST) for BLG solutions under the conditions studied [24]. The only exception is BSA with $LaCl_3$, in which no LLPS was found at our conditions studied. Here, the attractive forces are the weakest compared to the other systems studied and do not become strong enough to form LLPS, which is also reflected in the phase boundaries at lower $c_s$.

- **Role of solvent (isotope).** We observe a strong isotope effect for BSA in bulk solution, which was also shown in a previous investigation by Braun et al. [93], and the absence of a significant isotope effect for BLG illustrated in Fig. 2. The strength of solvent-solvent hydrogen bonds in $D_2O$ is increased compared to $H_2O$ [106], which leads to enhanced hydrophobic interactions within the protein stabilising and stiffening the protein structure [68, 69, 70, 71]. The hydrophobicity of a protein can be determined and expressed in multiple ways [107, 108]. One way is the Gibbs free energy of transfer from water, which is a direct method and was determined for BSA and BLG by Pérez-Fuentes et al. [72] (see Tab. 3). According to that, BSA is more hydrophobic than BLG [109, 110, 80, 111] meaning BSA will feel a stronger impact of $D_2O$. The hydrophobicity of a protein depends on its amino acid sequence, as well as its secondary structure. For $\alpha$-helix formation, hydrophobic amino acids are essential, since those provide stabilisation to the structure [67]. Thus, the presence and general nature of $\alpha$-helices contributes to the hydrophobicity of a protein and consequently to the amide isotope effect. In contrast, $\beta$-sheets show no isotope substitution and consequently no isotope effect [66]. BLG belonging to the protein class of all-$\beta$, therefore, will not undergo D/H isotope substitution for most of its structure compared to BSA belonging to the class of all-$\alpha$ (see Tab. 3) [112]. Thus, the difference between a strong isotope effect for BSA and its absence in BLG systems can be rationalised with its secondary structure/amino acid sequence and hydrophobicity as

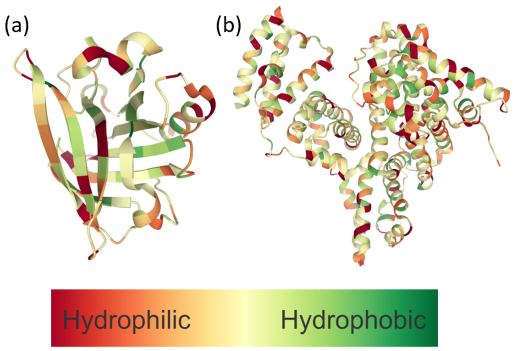


Figure 10: Hydrophobicity and 3D structure of proteins. These protein images of (a) BLG (PDB ID: 3PH6) [24] and (b) BSA (PDB ID: 4F5S) [113] are created with Mol* [114] on the RCSB PDB website (rcsb.org). The differences in secondary structure ($\alpha$-helices and $\beta$-sheets) are prominent (see also Tab. 3) and the colour code illustrates the hydrophobicity of different amino acids based on the work of Wimley and White [115]. Note that for better clarity BLG is illustrated only as a monomer.

illustrated in Fig. 10.

- **Role of anions.** There seems to be a fundamental difference in the ability to bind anions between BSA and BLG. We find that for BSA the anions impacted the BSA bulk phase behaviour differently depending on the anion type. The protein-salt interaction strength and contribution of anions to the phase boundaries increases from $Cl^- < NO_3^- < I^-$ [48], whereas for BLG all anions induce the same behaviour as shown in Fig. 2. The anion behaviour with BSA is in good agreement with literature from Carr et al. [116] and Longsworth et al. [76], which found that the number of anions bound per mole protein increases from $Cl^- < Br^- < NO_3^- < I^- = CNS^-$. Carr et al. [78] determined that 8 $Cl^-$ anions are bound to BSA at pH 5, but 12 $I^-$ ions. This effectiveness of specific binding of anions is similar for BLG [76], but reduced by a factor of 2 according to Longsworth et al. [76]. The parameter 'anion binding index' coined by Klotz et al. [75] illustrates the protein's affinity to bind anions. The anion binding index is 29 for serum albumin and 4.6 for beta-lactoglobulin (Tab. 3). This is

further supported by Tanford et al. [74] and the number of chloride ions bound by each protein. Chloride, in general, has a passive role [74, 73, 117] and is also not traceable in the BLG crystal structure [118, 24]. A recent study by Maier et al. [118] evaluated the surface coverage of cations on proteins of protein crystals after cation binding (here: $Y^{3+}$). In BLG, 30 % of its surface is covered with cations in comparison to only 15 % coverage for HSA meaning less space is available for anions to bind to BLG. Another explanation for the stronger anion binding of BSA might be the difference in binding mechanisms. BSA has a high affinity for anionic binding [119], whereas BLG prefers to bind hydrophobic molecules via hydrophobic interactions [79].

- **Re-entrant condensation.** Re-entrant condensation is driven by protein charge inversion and, beyond a certain concentration, consequently decreasing the attractive protein-protein interactions, which cause the cation-bridged protein clusters to break up [99]. In the presence of chloride salts, BSA and BLG undergo re-entrant condensation, as well as in the presence of iodide salts for BLG (shown in Fig. 2). For BSA with iodide salts, the samples stay in regime II upon increasing $c_s$ and do not redissolve, i.e. do not reach regime III (Fig. 1a,b of Ref. 48). In the systems with chloride salts, chloride has a passive role [117] and thus cations have the dominant role. In the system of BLG with iodide salts, BLG has in general a low anion binding affinity [75, 76], thus providing the mechanism for the occurrence of re-entrant condensation driven by multivalent cations. This behaviour changes for BSA with iodide salts. Iodide has a prominent role due to its protein stabilising role [120, 121], stronger binding to BSA [122], and a higher quantity bound to BSA [76, 116] than chloride. Additionally, an interplay between hydrophobic and charged amino acids improves anion binding to BSA [119, 123]. Thus, iodide induces stronger attractive protein-protein interactions and might facilitate anion-mediated protein cluster formation, which hinders re-entrant condensation.

Next, we focus on similarities and differences in protein *adsorption* of BSA and BLG on negatively charged and hydrophilic $SiO_2$:

- **Role of cation and anions.** The role of ions on the protein adsorption behaviour is reflected by its bulk properties. The stronger interactions an ion induces in bulk, the stronger is its effect on protein adsorption, in the sense that it enhances adsorption on $SiO_2$. One exception is BSA/$YI_3$, in which the combination of a strong cation with a strong anion seems to hinder each other.

- **Adsorption without salt.** Numerous studies have shown that BLG adsorption without salt is reduced compared to BSA [124, 125, 96], which is consistent with our findings. BLG has a smaller size (Tab. 3) and a higher surface charge density, which (probably) induces stronger repulsion in a system with negatively charge surfaces (proteins and substrate) and thus limiting surface adsorption.

- **Re-entrant adsorption.** The non-monotonic behaviour in adsorption at high $c_s$, i.e. decrease in adsorbed amount, can be observed for both proteins (Fig. 5 and 6 and in Ref. 48) and all salts in either solvent. Thus, we can conclude that it is related to the surface properties and not only to the bulk behaviour e.g. re-entrant condensation, which is absent for BSA with iodide salts in Ref. 48. Due to surface properties being hydrophilic and net negatively charged, anion binding is hindered and solely the cations and solvent are interacting with the surface. In the vicinity of the substrate (substrate and proteins are initially negatively charged), local charge inversion due to multivalent cation binding (i.e. stronger protein-interface repulsion) at high $c_s$ can be induced leading to re-entrant adsorption independent of the bulk properties.

- **Enhanced adsorption/Wetting transition.** In regime II, attractive interactions dominate the system, which induces enhanced adsorption compared to regime I and III in all systems studied (see Fig. 4 and

Table 4: Protein phase and adsorption behaviour. Properties and effects of BLG and BSA established in this work and previous studies of our group [48, 89, 88]. While the two proteins can show either temperature dependency, LCST and UCST, depending on the position in the phase diagram [126], they show the behaviour listed below under the conditions studied.

| **Protein behaviour** | BLG | BSA |
|---|---|---|
| LLPS | Two-step | One-step |
| Re-entrant condensation | √ | √ / X |
| Crystallisation | √ | X |
| Temperature dependency [127, 24, 60] | UCST | LCST |
| Isotope effect | X | √ |
| Anion effect | X | √ |
| Cation effect | √ | √ |
| Adsorption without salt | √ | √ |
| Re-entrant adsorption | √ | √ |
| Wetting transition | √ | √ |

8). The maximum adsorbed amount $d$ is limited by the strength of the cation/anion in the system and/or LLPS formation. In systems with LLPS, we observe continuous adsorption of proteins and the formation of a wetting layer at the bulk instability [89]. The general mechanism is explained in Ref. 89. This wetting transition discussed in Ref. 88, 89, 48 appears to be general, yet, the morphology of this wetting layer differed for BSA and BLG. In BSA, the wetting layer was diffuse with a high content of associated water trapped within [89] and in BLG, a densely packed layer formation can be observed (only 50 % hydration in Tab. 2). This difference could be speculated to be, under favourable conditions, the basis for the nucleation of protein crystals at interfaces in BLG systems and the absence of those in BSA systems, as well one has to bear in mind that BLG in its natural state forms dimers at the given pH[93].

## 4. Conclusions

In this study, we focus on the role of anions and solvents on the BLG behaviour in the bulk and at interfaces. We find that BLG is influenced less by the anion type or the solvent than BSA, which can be rationalised with its secondary structure (mainly $\beta$-sheets) and the properties of its amino acids and is consistent with literature showing a decreased affinity of BLG to bind anions in general compared to BSA [75, 76]. All phase diagrams established show re-entrant condensation and LLPS, which is induced by binding and bridging of multivalent cations. Through the addition of multivalent salts to the protein solution, protein adsorption increased at the interface up to a critical $c_s$, after which re-entrant adsorption occurred. The enhanced adsorption in regime II has been previously established for BSA [89] and illustrates the universality of a "wetting" transition at a bulk instability induced by LLPS formation. In addition, we find systematic differences between BSA and BLG and correlate those to their specific structure and properties. In the future, the combination of neutron and X-ray reflectivity may pave the way to study the transition from adsorption to crystallisation, i.e. nucleation at interfaces.

## CRediT authorship contribution statement

**Madeleine R. Fries:** Conceptualization, Methodology, Validation, Formal analysis, Investigation, Writing - Original draft preparation, Visualisation; **Maximilian W. A. Skoda:** Conceptualization, Methodology, Validation, Software, Formal analysis, Investigation, Resources, Data Curation, Writing, Visualisation; **Nina F. Conzelmann:** Formal analysis, Investigation; **Robert M. J. Jacobs:** Conceptualization, Methodology, Formal analysis, Investigation, Data Curation; **Ralph Maier:** Formal analysis, Investigation; **Niels Scheffczyk:** Formal analysis, Investigation; **Fajun Zhang:** Validation, Resources, Supervision; **Frank Schreiber:** Conceptualization, Project administration, Funding acquisition, Resources, Data Curation, Writing, Supervision.

## Declaration of Competing Interest

The authors declare that they have no known competing financial interests or personal relationships that could have appeared to influence the work reported in this paper.

## Data availability

The experimental data are available from the corresponding author on reasonable request.


## Acknowledgements

The authors thank Resul Akyüz and Alexander Krauth for their assistance in the experiments and the ISIS Biolab for granting us excess to the ATR-FTIR. Neutron beam time on the POLREF reflectometer was awarded by the ISIS Facility, experiment number RB1910571 (DOI: 10.5286/ISIS.E.RB1910571). Funding by Deutsche Forschungsgemeinschaft and instrument grant by Tübingen University/LISA$^+$ is gratefully acknowledged.


## Appendix A. Supporting Material

Supplementary data to this article can be found online at XXX.

## References


[1] P. Moughan, Digestion and absorption of proteins and peptides, in: Designing functional foods, Elsevier, 2009, pp. 148–170.

[2] S. Bilsborough, N. Mann, A review of issues of dietary protein intake in humans, International Journal of Sport Nutrition and Exercise Metabolism 16 (2) (2006) 129–152.

[3] G. H. Anderson, S. E. Moore, Dietary proteins in the regulation of food intake and body weight in humans, The Journal of Nutrition 134 (4) (2004) 974S–979S.

[4] Y. Guigoz, Dietary proteins in humans: basic aspects and consumption in switzerland, International Journal for Vitamin and Nutrition Research 81 (2-3) (2011) 87–100.

[5] J. Halkjaer, A. Olsen, L. Bjerregaard, G. Deharveng, A. Tjønneland, A. Welch, F. Crowe, E. Wirfält, V. Hellstrom, M. Niravong, et al., Intake of total, animal and plant proteins, and their food sources in 10 countries in the european prospective investigation into cancer and nutrition, European Journal of Clinical Nutrition 63 (4) (2009) S16–S36.

[6] G. Kontopidis, C. Holt, L. Sawyer, Invited review: $\beta$-lactoglobulin: binding properties, structure, and function, Journal of Dairy Science 87 (4) (2004) 785–796.

[7] M. D. Pérez, M. Calvo, Interaction of $\beta$-lactoglobulin with retinol and fatty acids and its role as a possible biological function for this protein: a review, Journal of Dairy Science 78 (5) (1995) 978–988.

[8] Q. Wang, J. C. Allen, H. E. Swaisgood, Binding of vitamin D and cholesterol to $\beta$-lactoglobulin, Journal of Dairy Science 80 (6) (1997) 1054–1059.

[9] S. Le Maux, S. Bouhallab, L. Giblin, A. Brodkorb, T. Croguennec, Bovine $\beta$-lactoglobulin/fatty acid complexes: binding, structural, and biological properties, Dairy Science & Technology 94 (5) (2014) 409–426.

[10] A. Mansouri, J.-L. Guéant, J. Capiaumont, P. Pelosi, P. Nabet, T. Haertlé, Plasma membrane receptor for beta-lactoglobulin and retinol-binding protein in murine hybridomas, Biofactors 7 (4) (1998) 287–298.

[11] H. Liu, W.-L. Chen, S. Mao, Antioxidant nature of bovine milk $\beta$-lactoglobulin, Journal of Dairy Science 90 (2) (2007) 547–555.

[12] G. Brignon, A. Chtourou, B. Ribadeau-Dumas, Does $\beta$-lactoglobulin occur in human milk?, Journal of Dairy Research 52 (2) (1985) 249–254.

[13] K.-M. Järvinen, P. Chatchatee, L. Bardina, K. Beyer, H. A. Sampson, IgE and IgG binding epitopes on $\alpha$-lactalbumin and $\beta$-lactoglobulin in cow's milk allergy, International Archives of Allergy and Immunology 126 (2) (2001) 111–118.

[14] Z. Teng, Y. Luo, Y. Li, Q. Wang, Cationic beta-lactoglobulin nanoparticles as a bioavailability enhancer: effect of surface properties and size on the transport and delivery in vitro, Food Chemistry 204 (2016) 391–399.

[15] Z. Teng, R. Xu, Q. Wang, Beta-lactoglobulin-based encapsulating systems as emerging bioavailability enhancers for nutraceuticals: a review, Rsc Advances 5 (44) (2015) 35138–35154.

[16] T. T. Reddy, L. Lavenant, J. Lefebvre, D. Renard, Swelling behavior and controlled release of theophylline and sulfamethoxazole drugs in $\beta$-lactoglobulin protein gels obtained by phase separation in water/ethanol mixture, Biomacromolecules 7 (1) (2006) 323–330.

[17] A. S. McAlpine, L. Sawyer, $\beta$-Lactoglobulin: a protein drug carrier?, Biochemical Society Transactions 18 (5) (1990) 879.

[18] Y. Mireille, I. van Hille, J.-P. Pélissier, P. Guilloteau, R. Toullec, In vivo milk digestion in the calf abomasum. II. Milk and whey proteolysis, Reproduction Nutrition Développement 24 (6) (1984) 835–843.

[19] R. S. Lam, M. T. Nickerson, Food proteins: a review on their emulsifying properties using a structure–function approach, Food Chemistry 141 (2) (2013) 975–984.

[20] W. Lohcharoenkal, L. Wang, Y. C. Chen, Y. Rojanasakul, Protein nanoparticles as drug delivery carriers for cancer therapy, BioMed Research International 2014 (2014) 180549.

[21] W. He, Y. Tan, Z. Tian, L. Chen, F. Hu, W. Wu, Food protein-stabilized nanoemulsions as potential delivery systems for poorly water-soluble drugs: preparation, in vitro characterization, and pharmacokinetics in rats, International Journal of Nanomedicine 6 (2011) 521.

[22] M. C. Yang, H.-H. Guan, J.-M. Yang, C.-N. Ko, M.-Y. Liu, Y.-H. Lin, Y.-C. Huang, C.-J. Chen, S. J. Mao, Rational design for crystallization of $\beta$-lactoglobulin and vitamin D3 complex: Revealing a secondary binding site, Crystal Growth and Design 8 (12) (2008) 4268–4276.

[23] A. L. Margolin, M. A. Navia, Protein crystals as novel catalytic materials, Angewandte Chemie International Edition 40 (12) (2001) 2204–2222.

[24] F. Zhang, G. Zocher, A. Sauter, T. Stehle, F. Schreiber, Novel approach to controlled protein crystallization through ligandation of yttrium cations, Journal of Applied Crystallography 44 (4) (2011) 755–762.

[25] A. Sauter, F. Roosen-Runge, F. Zhang, G. Lotze, A. Feoktystov, R. M. J. Jacobs, F. Schreiber, On the question of two-step nucleation in protein crystallization, Faraday Discussions 179 (2015) 41–58.

[26] A. Sauter, M. Oelker, G. Zocher, F. Zhang, T. Stehle, F. Schreiber, Non-classical pathways of protein crystallization in the presence of multivalent metal ions, Crystal Growth and Design 14 (12) (2014) 6357–6366.

[27] A. Sauter, F. Roosen-Runge, F. Zhang, G. Lotze, R. M. Jacobs, F. Schreiber, Real-time observation of nonclassical protein crystallization kinetics, Journal of the American Chemical Society 137 (4) (2015) 1485–1491.

[28] M. Elias, M. Laranjo, A. C. Agulheiro-Santos, M. E. Potes, The role of salt on food and human health, Salt in the Earth (2020) 19.

[29] R. Miller, R. Hoseney, Role of salt in baking, Cereal Foods World 53 (1) (2008) 4–6.

[30] S. Jeyarajah, J. C. Allen, Calcium binding and salt-induced structural changes of native and preheated $\beta$-lactoglobulin, Journal of Agricultural and Food Chemistry 42 (1) (1994) 80–85.

[31] M. E. Richert, G. G. Gochev, B. Braunschweig, Specific ion effects of trivalent cations on the structure and charging state of $\beta$-lactoglobulin adsorption layers, Langmuir 35 (35) (2019) 11299–11307.

[32] F. Zhang, F. Roosen-Runge, A. Sauter, R. Roth, M. W. A. Skoda, R. M. J. Jacobs, M. Sztucki, F. Schreiber, The role of cluster formation and metastable liquid-liquid phase separation in protein crystallization, Faraday Discussions 159 (2012) 313–325.

[33] J. Verran, Biofouling in food processing: biofilm or biotransfer potential?, Food and Bioproducts Processing 80 (4) (2002) 292–298.

[34] J. L. Nilsson, Fouling of an ultrafiltration membrane by a dissolved whey protein concentrate and some whey proteins, Journal of Membrane Science 36 (1988) 147–160.

[35] A. W. Mohammad, C. Y. Ng, Y. P. Lim, G. H. Ng, Ultrafiltration in food processing industry: review on application, membrane fouling, and fouling control, Food and Bioprocess Technology 5 (4) (2012) 1143–1156.

[36] W. Kunz, Specific ion effects in colloidal and biological systems, Current Opinion in Colloid & Interface Science 15 (1-2) (2010) 34–39.

[37] C. Spitzweg, A. E. Heufelder, J. C. Morris, Thyroid iodine transport, Thyroid 10 (4) (2000) 321–330.

[38] K. Berend, L. H. van Hulsteijn, R. O. Gans, Chloride: the queen of electrolytes?, European Journal of Internal Medicine 23 (3) (2012) 203–211.

[39] F. Ahad, S. A. Ganie, Iodine, iodine metabolism and iodine deficiency disorders revisited, Indian Journal of Endocrinology and Metabolism 14 (1) (2010) 13.

[40] Y. Efimova, A. Van Well, U. Hanefeld, B. Wierczinski, W. Bouwman, On the neutron scattering length density of proteins in $H_2O/D_2O$, Physica B: Condensed Matter 350 (1-3) (2004) E877–E880.

[41] A. Otsuki, L. De Campo, C. J. Garvey, C. Rehm, $H_2O/D_2O$ contrast variation for ultra-small-angle neutron scattering to minimize multiple scattering effects of colloidal particle suspensions, Colloids and Interfaces 2 (3) (2018) 37.

[42] E. A. Raymond, T. L. Tarbuck, M. G. Brown, G. L. Richmond, Hydrogen-bonding interactions at the vapor/water interface investigated by vibrational sum-frequency spectroscopy of $HOD/H_2O/D_2O$ mixtures and molecular dynamics simulations, The Journal of Physical Chemistry B 107 (2) (2003) 546–556.

[43] T. Sato, M. Hashizume, Y. Hotta, Y. Okahata, Morphology and proliferation of B16 melanoma cells in the presence of lanthanoid and $Al^{3+}$ ions, Biometals 11 (2) (1998) 107–112.

[44] J. Lettvin, W. Pickard, W. McCulloch, W. Pitts, A theory of passive ion flux through axon membranes, Nature 202 (4939) (1964) 1338–1339.

[45] C. R. Triggle, D. J. Triggle, An analysis of the action of cations of the lanthanide series on the mechanical responses of guinea-pig ileal longitudinal muscle, The Journal of Physiology 254 (1) (1976) 39–54.

[46] C. Aussel, R. Marhaba, C. Pelassy, J.-P. Breitmayer, Submicromolar $La^{3+}$ concentrations block the calcium release-activated channel, and impair CD69 and CD25 expression in CD3-or thapsigargin-activated Jurkat cells, Biochemical Journal 313 (3) (1996) 909–913.

[47] A. Zarros, A.-M. Byrne, S. D. Boomkamp, S. Tsakiris, G. S. Baillie, Lanthanum-induced neurotoxicity: solving the riddle of its involvement in cognitive impairment?, Archives of Toxicology 87 (11) (2013) 2031–2035.

[48] M. R. Fries, N. Conzelmann, L. Günter, O. Matsarskaia, M. W. A. Skoda, R. M. J. Jacobs, F. Zhang, F. Schreiber, Bulk phase behaviour vs. interface adsorption: I. specific multivalent cation and anion effects on bsa interactions, Langmuir 37 (1) (2021) 139–150.

[49] F. Zhang, M. W. A. Skoda, R. M. J. Jacobs, S. Zorn, R. A. Martin, C. M. Martin, G. F. Clark, S. Weggler, A. Hildebrandt, O. Kohlbacher, F. Schreiber, Reentrant condensation of proteins in solution induced by multivalent counterions, Physical Review Letters 101 (2008) 148101.

[50] I. Reviakine, D. Johannsmann, R. P. Richter, Hearing what you cannot see and visualizing what you hear: interpreting quartz crystal microbalance data from solvated interfaces, Analytical Chemistry 83 (2011) 8838–8848.

[51] M. V. Voinova, M. Rodahl, M. Jonson, B. Kasemo, Viscoelastic acoustic response of layered polymer films at fluid-solid interfaces: continuum mechanics approach, Physica Scripta 59 (5) (1999) 391.

[52] C. Steinem, A. Janshoff, Piezoelectric sensors, Vol. 5, Springer Science & Business Media, 2007.

[53] E. Rojas, M. Gallego, I. Reviakine, Effect of sample heterogeneity on the interpretation of quartz crystal microbalance data: impurity effects, Analytical Chemistry 80 (23) (2008) 8982–8990.

[54] K. K. Chittur, FTIR/ATR for protein adsorption to biomaterial surfaces, Biomaterials 19 (4-5) (1998) 357–369.

[55] A. Hughes, GitHub (2019). [link].
URL `https://github.com/arwelHughes/RasCAL_2019`

[56] M. Born, E. Wolf, Principles of Optics: Electromagnetic Theory of Propagation, Interference and Diffraction of Light, Cambridge University Press; 6th Edition, 1997.

[57] Névot, L., Croce, P., Caractérisation des surfaces par réflexion rasante de rayons x. application à l'étude du polissage de quelques verres silicates, Revue de Physique Appliquée (Paris) 15 (3) (1980) 761–779.

[58] D. Sivia, W. Hamilton, G. Smith, Analysis of neutron reflectivity data: maximum entropy, bayesian spectral analysis and speckle holography, Physica B: Condensed Matter 173 (1-2) (1991) 121–138.

[59] U. M. Elofsson, M. A. Paulsson, T. Arnebrant, Adsorption of $\beta$-Lactoglobulin A and B in relation to self-association: Effect of concentration and pH, Langmuir 13 (6) (1997) 1695–1700.

[60] O. Matsarskaia, M. K. Braun, F. Roosen-Runge, M. Wolf, F. Zhang, R. Roth, F. Schreiber, Cation-induced hydration effects cause lower critical solution temperature behavior in protein solutions, Journal of Physical Chemistry B 120 (31) (2016) 7731–7736.

[61] F. Roosen-Runge, F. Zhang, F. Schreiber, R. Roth, Ion-activated attractive patches as a mechanism for controlled protein interactions, Scientific Reports 4 (2014) 7016.

[62] O. Matsarskaia, F. Roosen-Runge, G. Lotze, J. Möller, A. Mariani, F. Zhang, F. Schreiber, Tuning phase transitions of aqueous protein solutions by multivalent cations, Physical Chemistry Chemical Physics 20 (42) (2018) 27214–27225.

[63] M. K. Braun, A. Sauter, O. Matsarskaia, M. Wolf, F. Roosen-Runge, M. Sztucki, R. Roth, F. Zhang, F. Schreiber, Reentrant phase behavior in protein solutions induced by multivalent salts: strong effect of anions $Cl^-$ versus $NO_3^-$, The Journal of Physical Chemistry B 122 (50) (2018) 11978–11985.

[64] F. Roosen-Runge, B. S. Heck, F. Zhang, O. Kohlbacher, F. Schreiber, Interplay of ph and binding of multivalent metal ions: charge inversion

and reentrant condensation in protein solutions, The Journal of Physical Chemistry B 117 (18) (2013) 5777–5787.

[65] M. K. Braun, M. Wolf, O. Matsarskaia, S. Da Vela, F. Roosen-Runge, M. Sztucki, R. Roth, F. Zhang, F. Schreiber, Strong isotope effects on effective interactions and phase behavior in protein solutions in the presence of multivalent ions, The Journal of Physical Chemistry B 121 (7) (2017) 1731–1739.

[66] B. A. Krantz, A. K. Srivastava, S. Nauli, D. Baker, R. T. Sauer, T. R. Sosnick, Understanding protein hydrogen bond formation with kinetic H/D amide isotope effects, Nature Structural Biology 9 (6) (2002) 458–463.

[67] M. Blaber, X. J. Zhang, B. W. Matthews, Structural basis of amino acid alpha helix propensity, Science 260 (5114) (1993) 1637–1640.

[68] Y. Efimova, S. Haemers, B. Wierczinski, W. Norde, A. v. Well, Stability of globular proteins in $H_2O$ and $D_2O$, Biopolymers: Original Research on Biomolecules 85 (3) (2007) 264–273.

[69] P. Cioni, G. B. Strambini, Effect of heavy water on protein flexibility, Biophysical Journal 82 (6) (2002) 3246–3253.

[70] G. C. Kresheck, H. Schneider, H. A. Scheraga, The effect of $D_2O$ on the thermal stability of proteins. Thermodynamic parameters for the transfer of model compounds from $H_2O$ to $D_2O$, The Journal of Physical Chemistry 69 (9) (1965) 3132–3144.

[71] M. J. Parker, A. R. Clarke, Amide backbone and water-related H/D isotope effects on the dynamics of a protein folding reaction, Biochemistry 36 (19) (1997) 5786–5794.

[72] L. Pérez-Fuentes, C. Drummond, J. Faraudo, D. Bastos-González, Interaction of organic ions with proteins, Soft Matter 13 (6) (2017) 1120–1131.

[73] R. K. Cannan, A. H. Palmer, A. C. Kibrick, The hydrogen ion dissociation curve of $\beta$-lactoglobulin, Journal of Biological Chemistry 142 (2) (1942) 803–822.

[74] C. Tanford, Interaction between proteins and chloride ion, in: Proceedings of the Iowa Academy of Science, Vol. 57, 1950, pp. 225–233.

[75] I. M. Klotz, J. M. Urquhart, The binding of organic ions by proteins. comparison of native and of modified proteins, Journal of the American Chemical Society 71 (5) (1949) 1597–1603.

[76] L. Longsworth, C. Jacobsen, An electrophoretic study of the binding of salt ions by $\beta$-lactoglobulin and bovine serum albumin., The Journal of Physical Chemistry 53 (1) (1949) 126–134.

[77] E. Brand, Amino acid composition of simple proteins, Annals of the New York Academy of Sciences 47 (2) (1946) 187–228.

[78] C. W. Carr, Studies on the binding of small ions in protein solutions with the use of membrane electrodes. IV. The binding of calcium ions in solutions of various proteins, Archives of Biochemistry and Biophysics 46 (2) (1953) 424–431.

[79] G. B. Jameson, J. J. Adams, L. K. Creamer, Flexibility, functionality and hydrophobicity of bovine $\beta$-lactoglobulin, International Dairy Journal 12 (4) (2002) 319–329.

[80] P.-Å. Albertsson, Partition between polymer phases, Journal of Chromatography A 159 (1) (1978) 111–122.

[81] C. Tanford, Hydrophobic free energy, micelle formation and the association of proteins with amphiphiles, Journal of Molecular Biology 67 (1) (1972) 59–74.

[82] S. H. Behrens, D. G. Grier, The charge of glass and silica surfaces, The Journal of Chemical Physics 115 (14) (2001) 6716–6721.

[83] R. Williams, A. M. Goodman, Wetting of thin layers of $SiO_2$ by water, Applied Physics Letters 25 (10) (1974) 531–532.

[84] M. Rodahl, P. Dahlqvist, F. Hook, B. Kasemo, The quartz crystal microbalance with dissipation monitoring (QCM-D), Biomolecular Sensors (2002) 304.

[85] G. Sauerbrey, Verwendung von Schwingquarzen zur Wägung dünner Schichten und zur Mikrowägung, Zeitschrift für Physik 155 (2) (1959) 206–222.

[86] K. Sakai, Quartz crystal microbalance with dissipation monitoring (QCM-D), in: Measurement Techniques and Practices of Colloid and Interface Phenomena, Springer, 2019, pp. 45–50.

[87] D. Johannsmann, The quartz crystal microbalance in soft matter research, Soft and Biological Matter (2015) 191–204.

[88] M. R. Fries, D. Stopper, M. K. Braun, A. Hinderhofer, F. Zhang, R. M. Jacobs, M. W. Skoda, H. Hansen-Goos, R. Roth, F. Schreiber, Multivalent-ion-activated protein adsorption reflecting bulk reentrant behavior, Physical Review Letters 119 (22) (2017) 228001.

[89] M. R. Fries, D. Stopper, M. W. Skoda, M. Blum, C. Kertzscher, A. Hinderhofer, F. Zhang, R. M. Jacobs, R. Roth, F. Schreiber, Enhanced protein adsorption upon bulk phase separation, Scientific Reports 10 (2020) 10349.

[90] S. X. Liu, J.-T. Kim, Application of Kevin—Voigt model in quantifying whey protein adsorption on polyethersulfone using QCM-D, JALA: Journal of the Association for Laboratory Automation 14 (4) (2009) 213–220.

[91] F. Höök, B. Kasemo, T. Nylander, C. Fant, K. Sott, H. Elwing, Variations in coupled water, viscoelastic properties, and film thickness of a mefp-1 protein film during adsorption and cross-linking: a quartz crystal

microbalance with dissipation monitoring, ellipsometry, and surface plasmon resonance study, Analytical Chemistry 73 (24) (2001) 5796–5804.

[92] T. Steiner, The hydrogen bond in the solid state, Angewandte Chemie International Edition 41 (1) (2002) 48–76.

[93] M. K. Braun, M. Grimaldo, F. Roosen-Runge, I. Hoffmann, O. Czakkel, M. Sztucki, F. Zhang, F. Schreiber, T. Seydel, Crowding-controlled cluster size in concentrated aqueous protein solutions: Structure, self- and collective diffusion, Journal of Physical Chemistry Letters 8 (12) (2017) 2590–2596.

[94] H. Susi, D. M. Byler, Fourier deconvolution of the amide I Raman band of proteins as related to conformation, Applied Spectroscopy 42 (5) (1988) 819–826.

[95] S. Ngarize, H. Herman, A. Adams, N. Howell, Comparison of changes in the secondary structure of unheated, heated, and high-pressure-treated $\beta$-lactoglobulin and ovalbumin proteins using Fourier transform Raman spectroscopy and self-deconvolution, Journal of Agricultural and Food Chemistry 52 (21) (2004) 6470–6477.

[96] B. Jachimska, S. Świątek, J. Loch, K. Lewiński, T. Luxbacher, Adsorption effectiveness of $\beta$-lactoglobulin onto gold surface determined by quartz crystal microbalance, Bioelectrochemistry 121 (2018) 95–104.

[97] G. Yohannes, S. K. Wiedmer, M. Elomaa, M. Jussila, V. Aseyev, M.-L. Riekkola, Thermal aggregation of bovine serum albumin studied by asymmetrical flow field-flow fractionation, Analytica Chimica Acta 675 (2) (2010) 191–198.

[98] S. Brownlow, J. H. M. Cabral, R. Cooper, D. R. Flower, S. J. Yewdall, I. Polikarpov, A. C. North, L. Sawyer, Bovine $\beta$-lactoglobulin at 1.8 Å resolution—still an enigmatic lipocalin, Structure 5 (4) (1997) 481–495.

[99] F. Zhang, M. W. Skoda, R. M. Jacobs, R. A. Martin, C. M. Martin, F. Schreiber, Protein interactions studied by saxs: effect of ionic strength and protein concentration for bsa in aqueous solutions, The Journal of Physical Chemistry B 111 (1) (2007) 251–259.

[100] H. A. Sober, Handbook of biochemistry: selected data for molecular biology, Chemical Rubber Co., 1968.

[101] T. Maruyama, S. Katoh, M. Nakajima, H. Nabetani, T. P. Abbott, A. Shono, K. Satoh, Ft-ir analysis of bsa fouled on ultrafiltration and microfiltration membranes, Journal of Membrane Science 192 (1-2) (2001) 201–207.

[102] L. R. Barbosa, M. G. Ortore, F. Spinozzi, P. Mariani, S. Bernstorff, R. Itri, The importance of protein-protein interactions on the pH-induced conformational changes of bovine serum albumin: a small-angle X-ray scattering study, Biophysical Journal 98 (1) (2010) 147–157.

[103] X. Arias-Moreno, O. Abian, S. Vega, J. Sancho, A. Velazquez-Campoy, Protein-cation interactions: structural and thermodynamic aspects, Current Protein and Peptide Science 12 (4) (2011) 325–338.

[104] R. G. Huber, J. E. Fuchs, S. von Grafenstein, M. Laner, H. G. Wallnoefer, N. Abdelkader, R. T. Kroemer, K. R. Liedl, Entropy from state probabilities: hydration entropy of cations, The Journal of Physical Chemistry B 117 (21) (2013) 6466–6472.

[105] P. J. Flory, Thermodynamics of high polymer solutions, The Journal of Chemical Physics 10 (1) (1942) 51–61.

[106] Y. Marcus, Ion properties, CRC Press, 1997.

[107] A. Mahn, M. E. Lienqueo, J. C. Salgado, Methods of calculating protein hydrophobicity and their application in developing correlations to predict hydrophobic interaction chromatography retention, Journal of Chromatography A 1216 (10) (2009) 1838–1844.

[108] M. E. Lienqueo, A. Mahn, J. A. Asenjo, Mathematical correlations for predicting protein retention times in hydrophobic interaction chromatography, Journal of Chromatography A 978 (1-2) (2002) 71–79.

[109] A. Kato, T. Matsuda, N. Matsudomi, K. Kobayashi, Determination of protein hydrophobicity using sodium dodecyl sulfate binding method, Journal of Agricultural and Food Chemistry 32 (2) (1984) 284–288.

[110] A. Kato, S. Nakai, Hydrophobicity determined by a fluorescence probe method and its correlation with surface properties of proteins, Biochimica et Biophysica Acta (BBA)-Protein structure 624 (1) (1980) 13–20.

[111] B. Hofstee, N. F. Otillio, Non-ionic adsorption chromatography of proteins, Journal of Chromatography A 159 (1) (1978) 57–69.

[112] A. D. Michie, C. A. Orengo, J. M. Thornton, Analysis of domain structural class using an automated class assignment protocol, Journal of Molecular Biology 262 (2) (1996) 168–185.

[113] A. Bujacz, Structures of bovine, equine and leporine serum albumin, Acta Crystallographica Section D: Biological Crystallography 68 (10) (2012) 1278–1289.

[114] D. Sehnal, A. Rose, J. Koča, S. Burley, S. Velankar, Mol*: towards a common library and tools for web molecular graphics, in: MolVa: Workshop on Molecular Graphics and Visual Analysis of Molecular Data, Brno, Czech Republic. Eurographics, 2018.

[115] W. C. Wimley, S. H. White, Experimentally determined hydrophobicity scale for proteins at membrane interfaces, Nature Structural Biology 3 (10) (1996) 842–848.

[116] C. W. Carr, Studies on the binding of small ions in protein solutions with the use of membrane electrodes. I. The binding of the chloride ion and other inorganic anions in solutions of serum albumin, Archives of Biochemistry and Biophysics 40 (2) (1952) 286–294.

[117] M. W. Washabaugh, K. D. Collins, The systematic characterization by aqueous column chromatography of solutes which affect protein stability., Journal of Biological Chemistry 261 (27) (1986) 12477–12485.

[118] R. Maier, G. Zocher, A. Sauter, S. Da Vela, O. Matsarskaia, R. Schweins, M. Sztucki, F. Zhang, T. Stehle, F. Schreiber, Protein crystallization in the presence of a metastable liquid-liquid phase separation, Crystal Growth and Design 20 (12) (2020) 7951–7962.

[119] Y. Nozaki, J. A. Reynolds, C. Tanford, The interaction of a cationic detergent with bovine serum albumin and other proteins, Journal of Biological Chemistry 249 (14) (1974) 4452–4459.

[120] M. Yamasaki, H. Yano, K. Aoki, Differential scanning calorimetric studies on bovine serum albumin: II. Effects of neutral salts and urea, International Journal of Biological Macromolecules 13 (6) (1991) 322–328.

[121] H. I. Okur, J. Hladilkova, K. B. Rembert, Y. Cho, J. Heyda, J. Dzubiella, P. S. Cremer, P. Jungwirth, Beyond the Hofmeister series: Ion-specific effects on proteins and their biological functions, The Journal of Physical Chemistry B 121 (9) (2017) 1997–2014.

[122] K. D. Collins, Ions from the hofmeister series and osmolytes: effects on proteins in solution and in the crystallization process, Methods 34 (3) (2004) 300–311.

[123] F. Karush, Heterogeneity of the binding sites of bovine serum albumin, Journal of the American Chemical Society 72 (6) (1950) 2705–2713.

[124] L. Pérez-Fuentes, C. Drummond, J. Faraudo, D. Bastos-González, Adsorption of milk proteins ($\beta$-casein and $\beta$-lactoglobulin) and BSA onto hydrophobic surfaces, Materials 10 (8) (2017) 893.

[125] B. Jachimska, K. Tokarczyk, M. Łapczyńska, A. Puciul-Malinowska, S. Zapotoczny, Structure of bovine serum albumin adsorbed on silica investi-

gated by quartz crystal microbalance, Colloids and Surfaces A: Physicochemical and Engineering Aspects 489 (2016) 163–172.

[126] N. Begam, O. Matsarskaia, M. Sztucki, F. Zhang, F. Schreiber, Unification of lower and upper critical solution temperature phase behavior of globular protein solutions in the presence of multivalent cations, Soft Matter 16 (8) (2020) 2128–2134.

[127] A. C. Dumetz, A. M. Chockla, E. W. Kaler, A. M. Lenhoff, Protein phase behavior in aqueous solutions: crystallization, liquid-liquid phase separation, gels, and aggregates, Biophysical Journal 94 (2) (2008) 570–583.

# *Supporting Material*: Bulk phase behaviour vs interface adsorption: Effects of anions and isotopes on BLG interactions

Madeleine R. Fries

*Institute for Applied Physics, University of Tübingen, 72076 Tübingen, Germany, email: madeleine.fries@uni-tuebingen.de*

Maximilian W. A. Skoda

*ISIS Facility, STFC, Rutherford Appleton Laboratory, Didcot, OX11 0QX, United Kingdom, email: maximilian.skoda@stfc.ac.uk*

Nina F. Conzelmann

*Institute for Applied Physics, University of Tübingen, 72076 Tübingen, Germany, email: nina.conzelmann@student.uni-tuebingen.de*

Robert M. J. Jacobs

*Department for Chemistry, University of Oxford, Oxford, OX1 3TA, United Kingdom, email: robert.jacobs@chem.ox.ac.uk*

Ralph Maier

*Institute for Applied Physics, University of Tübingen, 72076 Tübingen, Germany, email: ralph.maier@uni-tuebingen.de*

Niels Scheffczyk

*Institute for Applied Physics, University of Tübingen, 72076 Tübingen, Germany, email: niels.scheffczyk@student.uni-tuebingen.de*

Fajun Zhang

*Institute for Applied Physics, University of Tübingen, 72076 Tübingen, Germany, email: fajun.zhang@uni-tuebingen.de*

Frank Schreiber*

*Institute for Applied Physics, University of Tübingen, 72076 Tübingen, Germany, email: frank.schreiber@uni-tuebingen.de*

*Corresponding author, email: frank.schreiber@uni-tuebingen.de, telephone: 0049-7071-29-76058, fax: 0049-7071-29-5110

**Abstract**

Experimental procedures and additional experimental data supporting the main findings of this paper are explained in the following. The Supporting Material are structured as follows:

**Sections:** S1 to S4

**Pages:** S1 to S8

**Figures:** S1 to S6

**Table:** S1

---

## S1. Determination of the protein phase behaviour

The phase diagrams shown in Fig. 1 (main text) were predominately produced by visual inspection of dilution series. An example of a dilution series of BLG with $LaCl_3$ and $LaI_3$ in $H_2O$ is given in Fig. S1.

At low $c_p$ (i.e. 5 mg/ml), the determination of the phase transition by visual inspection was not precise enough and UV-vis transmittance measurements were performed as shown in Fig. S2. The consequential determined values of $c^*$ and $c^{**}$ are listed in Tab. 1 (main text).

## S2. Effect of pH on bulk behaviour

In order to assess and estimate the change in pH induced by the addition of multivalent salts, pH measurements were conducted in Fig. S3 with the pH/Ion meter S220 of Seven Compact series from Mettler Toledo (USA). The precision of this method can be estimated to be around $\pm$ 0.1 considering deviations in pipetting and electrode precision. Initially for both systems, the pH slightly decreases due to the salt-induced water hydrolysis upon the addition of salts [1], yet these changes do not correlate with the phase behaviour and can not explain phenomena such as re-entrant condensation at high $c_s$. Consequently, pH can be excluded as the dominant force driving the bulk phase behaviour. This is in good agreements with past pH measurements with BLG and other globular, net negatively charged proteins [1].


Figure S1: Phase transitions. Dilution series at 5 mg/ml BLG and at room temperature with (a) $LaCl_3$ and (b) $LaI_3$ in $H_2O$. The bottles are labelled with the respective $c_s$ in mM.

## S3. QCM-D data of solvent exchange ($H_2O/D_2O$)

In Fig. S4, an example of an adsorption process of a sample containing 5 mg/ml BLG with $LaCl_3$ in $H_2O$ and $D_2O$ is plotted. The raw data is analysed with a viscoelastic model with the fitting parameters listed in Tab. S1 to extract the adsorbed layer thickness $d$. The analysed data can be found in the main text in Fig. 5.

## S4. NR data

In Fig. S5, the Bayesian error analysis (confidence interval of 95 %) of the individual fitted reflectivity curves and SLDs with 5 mg/ml BLG in $D_2O$ and $H_2O$ in the presence of $LaCl_3$ are shown and respectively for $LaI_3$ shown in Fig. S6. The extracted thicknesses, roughnesses and hydrations are listed in the main text in Tab. 2.

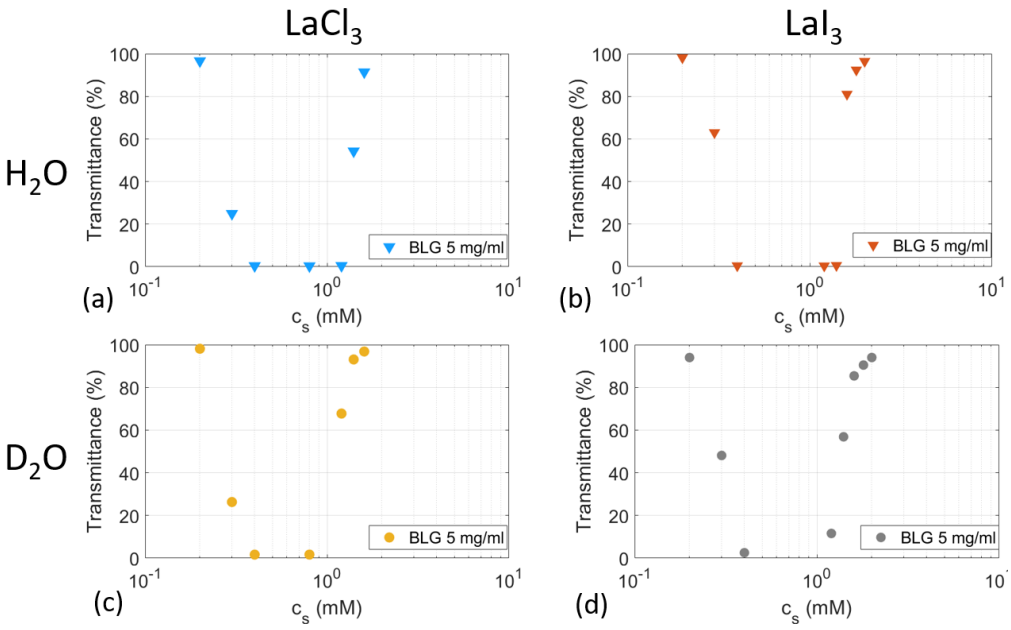


Figure S2: UV-vis transmittance measurements. The phase transitions at 5 mg/ml BLG with $LaCl_3$ (a) in $H_2O$, (c) in $D_2O$, and BLG with $LaI_3$ (b) in $H_2O$, (d) in $D_2O$ are depicted dependent on its transmittance ($\lambda$ = 400 - 800 nm). $c^*$ is defined as the $c_s$, at which transmittance starts to decrease. $c^{**}$ is defined as $c_s$ at which 50 % of transmittance is restored. The absolute numbers are listed in Tab. 1.

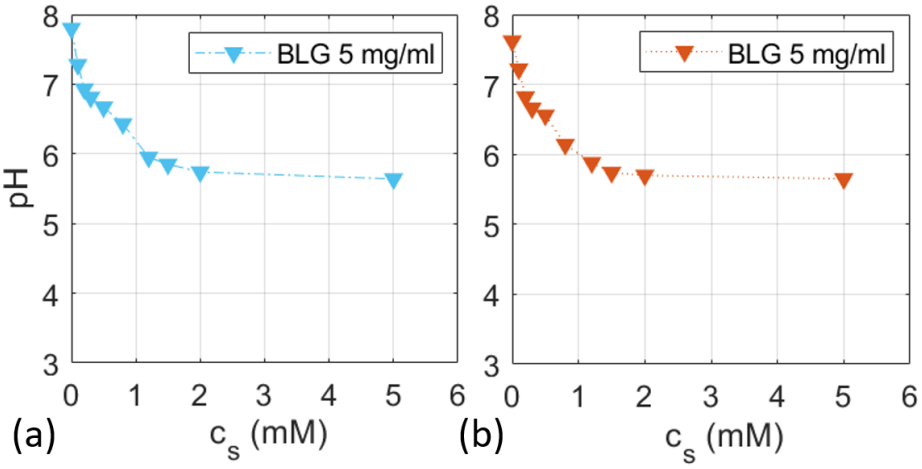


Figure S3: Bulk pH measurements at 5 mg/ml BLG with (a) $LaCl_3$ and (b) $LaI_3$ in $H_2O$ at room temperature. No salt-type-dependent differences in pH can be observed.

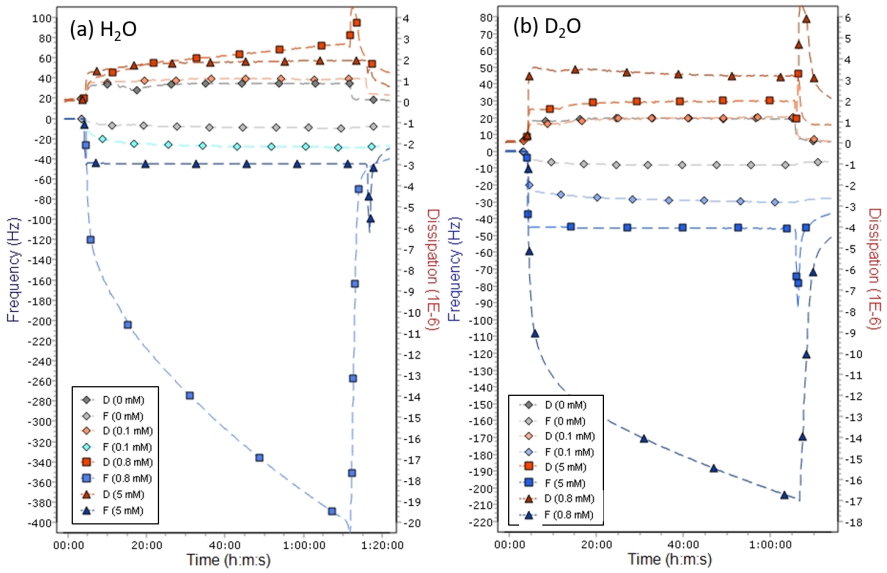


Figure S4: Raw QCM-D data. Frequency (blue) and dissipation (red) of the $9^{th}$ overtone of BLG at 5 mg/ml with $LaCl_3$ (a) in $H_2O$ and (b) $D_2O$ at 0, 0.1, 0.8, and 5 mM $c_s$. These $c_s$ cover the individual regimes. The measurements are calibrated and started in $H_2O$. After a few minutes, the salt/water mixture is pump into the cell inducing protein adsorption. After roughly 1 h, the cell is flushed with $H_2O$ to check for the reversibility of protein adsorption. Note that spikes in the raw data are induced by turning the pump on and off for solution exchange.

Table S1: Material properties. Fitting constants for QCM-D data modelling [2, 3].

| **Material** | **Density (g/L)** | **Viscosity (kg/(m·s))** |
|---|---|---|
| BLG in $H_2O$ (5 mg/ml) | 998 | 0.00101 |
| BLG in $D_2O$ (5 mg/ml) | 1106 | 0.00125 |
| BLG (powder) | 1320 | - |
| Adsorbed monolayer in $H_2O$ (1 ML) | 1200 | - |
| Adsorbed monolayer in $D_2O$ (1 ML) | 1250 | - |

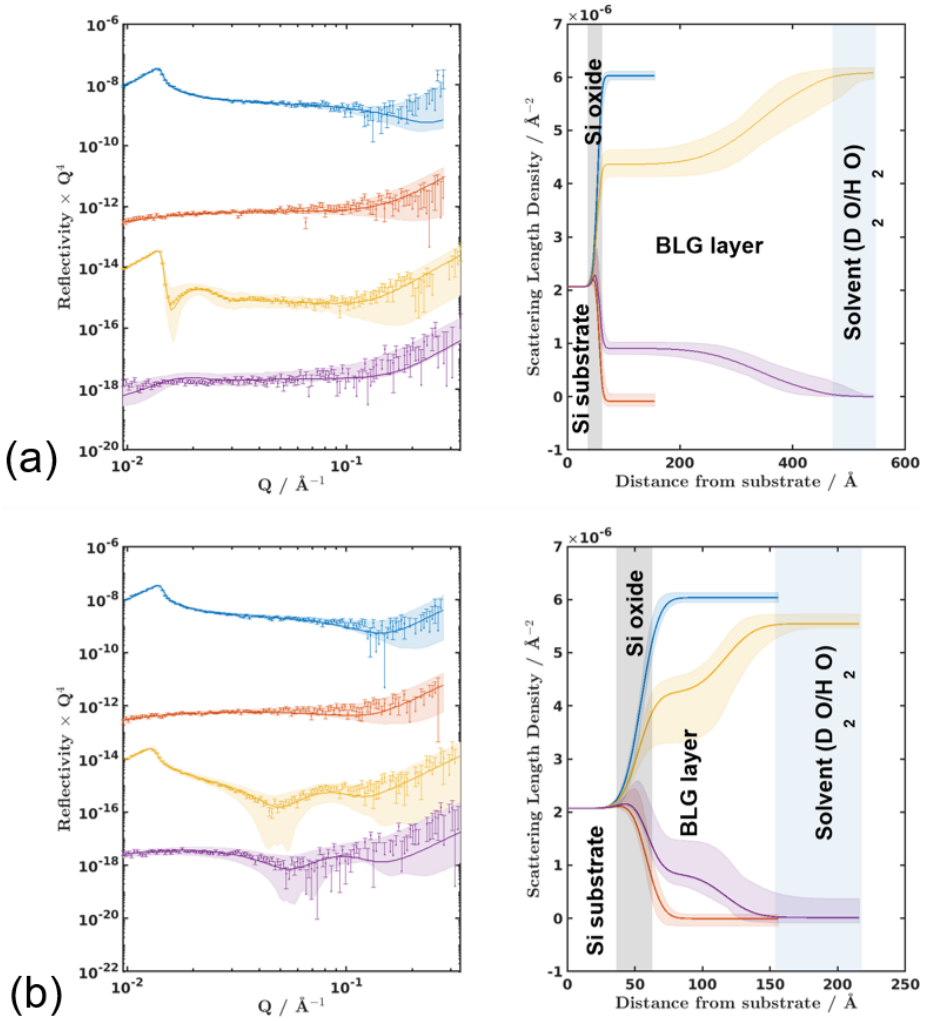


Figure S5: Bayesian Error Analysis. Fit quality of model showing 95 % confidence intervals (shaded regions) of the generated reflectivity curves (left) and the resulting scattering length density profiles (right). The data shown is BLG at 5 mg/ml without salt (blue and red, dashed) as a reference and (a) in regime II (i.e. 0.8 mM $LaCl_3$) and (b) in regime III (i.e. 5 mM $LaCl_3$) (yellow and purple, solid) in $D_2O$ and $H_2O$, respectively.

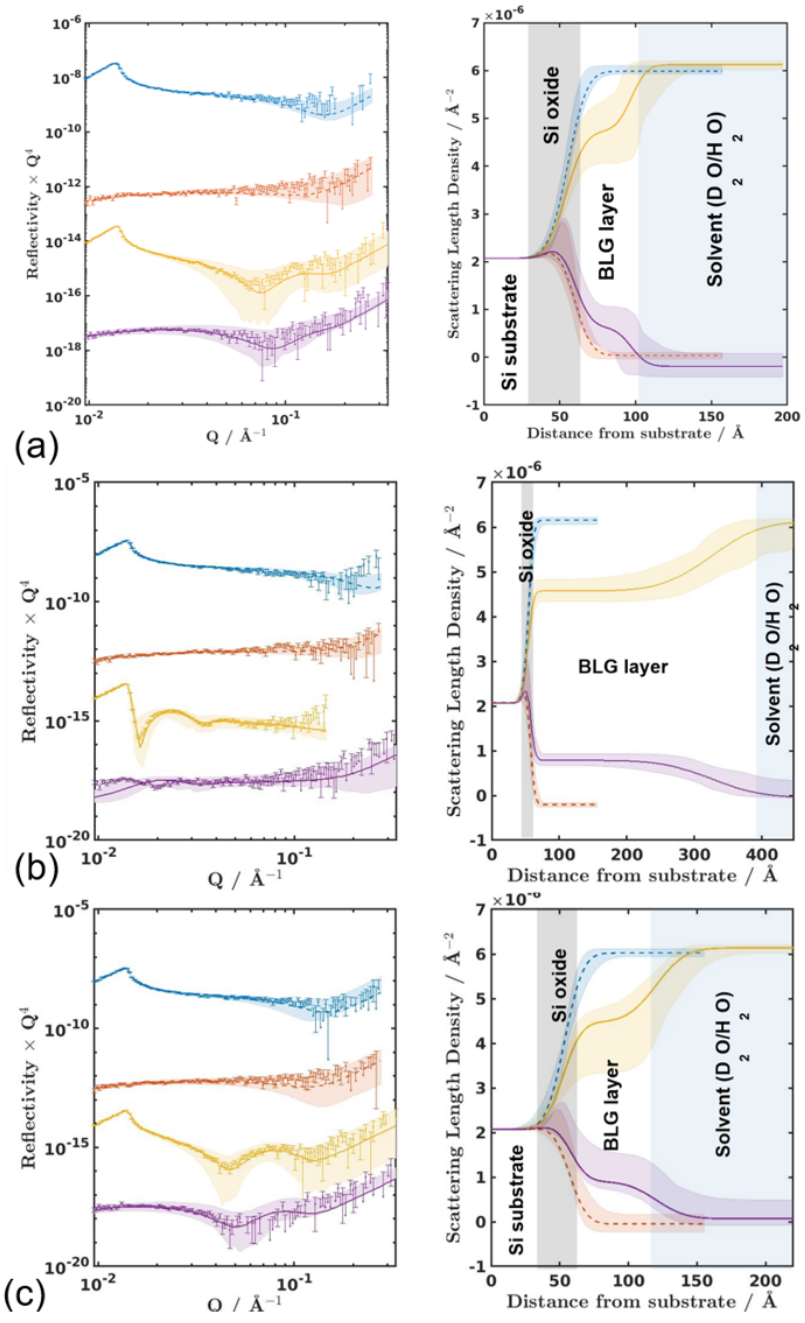


Figure S6: Bayesian Error Analysis. Fit quality of model showing 95 % confidence intervals (shaded regions) of the generated reflectivity curves (left) and the resulting scattering length density profiles (right). The data shown is BLG at 5 mg/ml without salt (blue and red, dashed) as a reference and (a) in regime I (0.1 mM $LaI_3$), (b) in regime II (i.e. 0.8 mM $LaI_3$) and (c) in regime III (i.e. 5 mM $LaI_3$) (yellow and purple, solid) in $H_2O$ and $D_2O$, respectively.

## References


[1] F. Roosen-Runge, B. S. Heck, F. Zhang, O. Kohlbacher, F. Schreiber, Interplay of ph and binding of multivalent metal ions: charge inversion and reentrant condensation in protein solutions, The Journal of Physical Chemistry B 117 (18) (2013) 5777–5787.

[2] J. Crittenden, R. Trussell, D. Hand, K. Howe, G. Tchobanoglous, Appendix c: Physical properties of water, MWH's Water Treatment: Principles and Design (2012) 1861–1862.

[3] J. Kim, N. Weber, G. Shin, Q. Huang, S. Liu, The study of $\beta$-lactoglobulin adsorption on polyethersulfone thin film surface using qcm-d and afm, Journal of Food Science 72 (4) (2007) E214–E221.